DISSERTATIONS IN
FORESTRY AND
NATURAL SCIENCES

Timo Lähivaara

Discontinuous Galerkin Method for Time-Domain Wave Problems

Publications of the University of Eastern Finland
Dissertations in Forestry and Natural Sciences

UNIVERSITY OF
EASTERN FINLAND

TIMO LÄHIVAARA

Discontinuous Galerkin method for time-domain wave problems

Publications of the University of Eastern Finland
Dissertations in Forestry and Natural Sciences
No 18

Academic Dissertation
To be presented by permission of the Faculty of Science and Forestry for public examination in the Auditorium ML2 in Medistudia Building at the University of Eastern Finland, Kuopio, on December, 11, 2010,
at 12 o'clock noon.

Department of Physics and Mathematics

Kopijyvä
Kuopio, 2010
Editors: Prof. Pertti Pasanen,
Dr. Sinikka Parkkinen, Prof. Kai Peiponen

Distribution:
University of Eastern Finland Library / Sales of publications
P.O. Box 107, FI-80101 Joensuu, Finland
tel. +358-50-3058396
http://www.uef.fi/kirjasto

ISBN: 978-952-61-0239-9
ISSN: 1798-5668
ISSNL: 1798-5668
ISBN: 978-952-61-0240-5 (PDF)
ISSN: 1798-5676 (PDF)

Author's address:
University of Eastern Finland
Department of Physics and Mathematics
P.O. Box 1627
70211 Kuopio
Finland
email: timo.lahivaara@uef.fi

Supervisors:
Docent Tomi Huttunen, PhD
University of Eastern Finland
Department of Physics and Mathematics
Finland
email: tomi.huttunen@uef.fi

Professor Jari Kaipio, PhD
University of Eastern Finland
Department of Physics and Mathematics
Finland
email: jari@math.auckland.ac.nz

Reviewers:
Professor Jan Hesthaven, PhD
University of Brown
Division of Applied Mathematics
United States of America
email: jan.hesthaven@brown.edu

Docent Leo Kärkkäinen, PhD
Nokia Research Center
Finland
email: leo.m.karkkainen@nokia.com

Opponent:
Docent Jari Toivanen, PhD
University of Jyväskylä
Department of Mathematical Information
Technology
Finland
email: toivanen@stanford.edu

ABSTRACT

Time-dependent wave fields are often approximated using wave equations. Due to the oscillatory nature of wave phenomena, numerical approximations of wave equations are challenging. Approximating wave problems with tolerable accuracy requires the use of a relatively dense spatial discretization. For standard numerical techniques, such as the low-order finite difference and finite element methods, 10 grid points per wavelength is considered the rule of thumb. Particularly for short wavelengths, the requirement of a dense mesh can easily lead to problems of intolerable computational complexity. The computational burden can, however, be reduced using more sophisticated numerical methods. Discontinuous Galerkin (DG) methods to address this issue have been extensively studied.

In this thesis, the DG method is used for modeling time-dependent wave fields in an inhomogeneous medium. More precisely, the main focus was to develop a feasible DG method for modeling wave fields with complicated geometries with reduced computational complexity. The DG approach was examined for unbounded two- and three-dimensional wave problems. Truncation of a physically unbounded problem into a problem with a bounded domain affects the accuracy of the numerical solution. A perfectly matched layer is used to truncate the computational domain in three-dimensional wave problems.

In the numerical experiments, the DG method was studied from a computational point of view. Based on previous theoretical analyses, non-uniform basis orders to increase the accuracy of the numerical solution was the main research topic. The non-uniform basis orders were investigated in two- and three-dimensional problems. In the model problems, non-uniform basis orders were also extended to a case in which wave propagation and scattering were studied in a geometry that comprised a loudspeaker. In this model problem, the numerical solution was compared to actual measurements. The results predicted that a predetermined error level of the solution can be obtained with the correct basis order choices. At the same time, the use of non-uniform basis orders reduces the computational load.

AMS Classification: 65M60, 65Z05, 74J05, 74J20, 74S30, 76Q05

Universal Decimal Classification: 519.6, 534-8, 534.2

INSPEC Thesaurus: acoustic waves; acoustics; numerical analysis; time-domain analysis; modelling

Yleinen suomalainen asiasanasto: aaltoliike; akustiikka; numeeriset menetelmät; numeerinen analyysi; matemaattiset mallit; mallintaminen

ACKNOWLEDGMENTS

The work for this thesis was performed at the Department of Physics in the University of Kuopio during the years 2006-2009.

I wish to express my gratitude to my principal supervisor, Docent Tomi Huttunen, for suggesting this interesting topic to me and for providing tireless guidance during the project. I am also very grateful to my other supervisor, Professor Jari Kaipio, for providing me the opportunity to work with his research group and for his excellent comments for improving the thesis. Also, I give special thanks to Doctor Simo-Pekka Simonaho for friendship and for providing all the experimental measurements used in this thesis.

In the final steps of finishing this thesis, the official pre-examiners, Professor Jan Hesthaven and Docent Leo Kärkkäinen, provided excellent suggestions and comments for improving the manuscript.

Along with the faculty and staff of the Department of Physics, I wish to thank Kati Niinimäki for friendship and scientific discussion. Also, I wish to thank Aki Pulkkinen who has patiently taught me computer programming and for several excellent comments related to the results of this thesis. I wish to thank Doctor Mauri Puoskari for solving all my computer-related problems.

Naturally, I am grateful to my parents, Hannu Mönkkönen and Sisko Lähivaara, and also to my brother Tero Lähivaara and his family. Also, I wish to thank my very good friends Marko, Kirsi, Piia, Mikko, Pasi, Henri, and Joni-Pekka for teaching me several things in life. Last, but not least, my deepest appreciation goes to my common-law wife Saara.

This study was supported by the Finnish Funding Agency for Technology and Innovation, the European Regional Development Fund, the Finnish IT Center for Science, the Cultural Foundation of Northern Savo, the Academy of Finland (the Finnish Programme for Centres of Excellence in Research 2006-2011), the Emil Aaltonen foundation, and the Foundation for Advanced Technology of Eastern Finland.

Saatanan saatana, kun menee hyvä mies pilalle
Urho Kaleva Kekkonen (1900 – 1986)

Kuopio November 7, 2010 *Timo Lähivaara*

ABBREVIATIONS

2D	Two-dimensional
3D	Three-dimensional
ABC	Absorbing boundary condition
ADER	Arbitrary high-order derivatives
AHOC	Arbitrary high-order absorbing boundary condition
BEM	Boundary element method
CFL	Courant-Friedrichs-Lewy number
CN	Crank-Nicolson
CSC	IT Center for Science
DG	Discontinuous Galerkin
DOF	Degrees of freedom
ESDIRK4	Fourth-order explicit, singly diagonally implicit Runge-Kutta
error	Relative error
FD	Finite difference
FDTD	Finite difference time-domain
FE	Finite element
FEM	Finite element method
FV	Finite volume
FVM	Finite volume method
GB	Gigabyte
GPR	Ground-penetrating radar
GPU	Graphics processing unit
HLL	Harten-Lax-van Leer
IBV	Initial-boundary value
LSRK	Low-storage Runge-Kutta
LTS	Local time-stepping
MPI	Message passing interface
MPP	Massively parallel processor
PC	Personal computer
PDE	Partial differential equation
PML	Perfectly matched layer
RAM	Random access memory
RK	Runge-Kutta
UWVF	Ultra-weak variational formulation

NOMENCLATURE[1]

$a \pm \Delta a$	Slope of the line, 5.1.2
a_1, a_2	Parameters for Ricker wavelet, 5.1.2
A	Matrix for hyperbolic system, 3.1
A_1, A_2, A_3	Matrices for hyperbolic system, 3.1
$b \pm \Delta b$	Axis-intercept of the line, 5.1.2
B	Matrix for hyperbolic system, 3.1
c	Speed of sound, 2.2
c^-, c^+	Wave speeds in neighboring elements, 4.2
d_0	Parameter for PML, 3.3
$d_{x_1}, d_{x_2}, d_{x_3}$	PML parameters, 3.3
D	Boundary matrix, 4.2
$D^+, D^-, D^+_\sigma, D^-_\sigma$	Boundary flux matrices, 4.2
f	Frequency, 5.1
g	Boundary source term, 2.3
$\boldsymbol{g}$	Vector, 4.2
G	Auxiliary variable, 3.3
$h, h_{\min}, h_{\max}$	Mesh parameters, 3.5, 4.4, 5.1
i	Imaginary unit $\sqrt{-1}$, 3.3
j	Integer
k	Wave number, 5.1.2
$\boldsymbol{k}$	Vector, 5.1.1
ℓ	Integer
$\boldsymbol{l}^+, \boldsymbol{l}^-$	Vectors, 4.2
m	Integer
n	Normal vector, 2.3
n_{el}	Number of elements, 5.1.3
n_p	Number of partitions, 5.1
n^+, n^-	Normal vectors, 2.3
N	Number of finite elements, 4.2
$\mathcal{N}$	Boundary matrix, 4.2
p	Order of basis functions, 3.5
$\boldsymbol{q}_1, \boldsymbol{q}_2, \boldsymbol{q}_3$	Vectors, 3.3
Q	Boundary condition parameter, 2.3
s	Source function parameter, 5.1.1
S	Coupling matrix, 4.2
S_s	Entropy, 2.2
t	Time variable, 2.1

[1]The number at the end of a line shows the section in which the symbol is first used.

t_0	Source function parameter, 5.2
$\top$	Transpose, 4.2
u	Acoustic pressure, 2.1
u_0	Ambient pressure, 2.1
u_{i1}, u_{i2}	Initial conditions, 2.3
u_n	Numerical solution, 5.1.1
u_e	Analytic solution, 5.1.1
u^+, u^-	Acoustic pressures, 2.3
$\boldsymbol{u}$	Vector, 3.1
$\mathfrak{U}$	Pressure, 2.1
$\boldsymbol{v}$	Test function, 4.2
$\boldsymbol{\nu}$	Particle velocity, 2.1
$\boldsymbol{\nu}_0$	Ambient particle velocity, 2.1
$\boldsymbol{\nu}^+, \boldsymbol{\nu}^-$	Particle velocities, 2.3
x_0	Starting position for PML damping, 3.3
x_s	Source function parameter, 5.1.3
x_1, x_2, x_3	Spatial variables, 2.1
$\boldsymbol{x}$	Spatial variable, 2.1
$\boldsymbol{x}_{CM}^m$	Position of the centroid of the m'th tetrahedra, 5.1.2
$\boldsymbol{x}_\ell^m$	Vertices of the m'th tetrahedra, 5.1.2
α	Parameter for initial condition, 5.1.3
β	Absorption coefficient, 3.1
γ	Source function parameter, 5.2
Γ^t	Domain boundary, 2.3
Γ	Exterior boundary of the computational domain, 2.3
Γ_i	Adjacent element boundary, 4.2
Γ_e	Exterior boundary part of the element, 4.2
δ_t	Time step length, 3.5
η	Power parameter for PML, 3.3
ϑ	PML thickness, 3.3
σ	Flux coupling parameter, 2.3, 4.2
ρ	Ambient density, density, 2.1
ξ	Acoustic part of density, 2.1
ϱ	Mass density, 2.1
$\mathcal{O}$	Error function, 4.4
κ	Free parameter, 5.1.2
λ	Wavelength, 5.1.2
ω	Angular frequency, 3.3
Ω	Computational domain, 2.3
Ω^+, Ω^-	Computational domains, 2.3

LIST OF PUBLICATIONS

This thesis consists of an overview and the following four original articles, which are referred to in the text by their Roman numerals **I-IV**:

I T. Lähivaara, M. Malinen, J. P. Kaipio, and T. Huttunen. Computational aspects of the discontinuous Galerkin method for the wave equation. *Journal of Computational Acoustics*, 16(4):507-530, 2008.

II T. Lähivaara and T. Huttunen. A non-uniform basis order for the discontinuous Galerkin method of the acoustic and elastic wave equations. *Applied Numerical Mathematics*, Accepted for publication, 2010.

III T. Lähivaara and T. Huttunen. A non-uniform basis order for the discontinuous Galerkin method of the 3D dissipative wave equation with perfectly matched layer. *Journal of Computational Physics*, 229(13):5144-5160, 2010.

IV S-P. Simonaho, T. Lähivaara, and T. Huttunen. Modeling of acoustic wave propagation in time-domain using the discontinuous Galerkin method - a comparison with measurements. Submitted for publication.

AUTHOR'S CONTRIBUTION

All publications are a result of collaborations with co-authors. The author was the principal writer for publications **I**,**II**, and **III**. In all published papers, the author of this thesis was responsible for developing the methods presented in the publications, and implemented the numerical simulations and computed results in the C/C++, Comsol Multiphysics®, Gambit®, and Matlab® platforms. The Matlab® software was used mainly for visualization. In publication **IV**, the writing was divided equally among the authors of the paper. The author of this thesis performed the numerical simulations and computed results presented in publication **IV**.

Contents

1 Introduction

In several fields of computational physics and engineering, it is extremely challenging to model mechanical wave problems in the time-domain. Only the simplest problems can be solved analytically and the performance of standard numerical methods for hyperbolic partial differential equations (PDEs), such as acoustic and elastic wave equations and Maxwell's equations, depends on the wavelength of the sound field. Particularly at high frequencies, the requirement of a certain number of discretization points per wavelength often leads to an impractical computational task. On the other hand, when the grid density is increased, the length of the time step must be decreased to obtain an accurate solution in terms of time integration.

There is a clear need for accurate methods for modeling wave fields in the time-domain in complex geometries. Applications for modeling mechanical time-domain wave fields are, for example, non-destructive testing, exploration seismology, electromagnetics, and medical ultrasonics. During the last few decades, several approaches have been proposed to obtain stable, accurate, computer-friendly, and fast methods to use for numerically approximating the corresponding initial-boundary value problems. Traditional full-wave approaches that have been used for this are the finite difference (FD) [1] and finite element (FE) [2] methods.

Finite difference methods for the wave problems are limited by the requirement for a dense spatial discretization and are therefore computationally demanding at high frequencies. On the other hand, modeling of wave fields in complex geometries with different boundary models using FD methods is challenging. Despite the disadvantages of the FD methods, they are still extensively studied and several recent reports have been published [3,4]. The motivation for using the FD approach is the simplicity of the method. The discretization of the studied initial-boundary value problem can be easily achieved.

The FE method is a more flexible method than the FD approach for approximating the wave problems. The FE method can handle complex geometries. When using low-order FE methods, however, the demand for dense meshes can be computationally intolerable. Ten points per wavelength is considered the rule of thumb. Despite the disadvantages, the FE method is a widely used tool for approximating wave propagation in several fields of physics and engineering and is considered the standard method for full-wave simulations. Wave propagation problems are solved

using the FE method in several reports (see [2,5]).

A promising approach for accurately approximating mechanical wave fields is the discontinuous Galerkin (DG) method [6]. The DG method has several features that make it an attractive candidate for large-scale wave simulations. The variational formulation reduces each element of the computational mesh to a subproblem. With the DG method, the communication between adjacent elements is handled using the transmission condition (known as numerical flux [7]). On the other hand, the variational form allows for easier parallelization of the solver code and the material parameters, the order of the basis functions, and the length of the time step can be chosen individually for each subproblem. Of course, there are also drawbacks when using DG methods. For example, high-order basis functions force the use of small time steps, which is time consuming [7], and there are stability problems with the high-order basis functions used with the small elements of the computational mesh.

Factors other than the method used for spatial discretization affect the accuracy of the domain-based full-wave methods. These include the truncation of a physically unbounded problem into a problem with a bounded domain. Namely, the effect of the boundary condition on the auxiliary exterior boundary of the bounded domain should allow waves to propagate outward without numerical reflections back into the domain. The use of the Engquist-Majda type absorbing boundary condition [8] affects the accuracy of the solutions because unwanted numerical reflections arise from the boundaries. One promising approach for reducing these numerical reflections is to use the perfectly matched layer (PML) [9] to truncate the effect of the solution on the boundaries. Generally, the PML is a numerical damping layer and was originally published by Bérenger in [9] for electromagnetic waves.

The time integration method used for approximating the time derivatives has a great impact on the accuracy of the numerical solution. During the last few decades, several implicit and explicit approaches have been explored to obtain a fast and stable time integration method. These include the Runge-Kutta methods [10–13], the Newmark method [14], and the ADER time integration approach using arbitrary high-order derivatives [15,16].

Aims and content of this thesis

In this thesis, the DG method, originally published by Reed and Hill in [6], was implemented for acoustic wave problems in inhomogeneous media. The DG method was implemented using the C/C++ programming lan-

guage and solver parallelization with the message passing interface (MPI). The main focus was on the development of a DG method that is feasible for practical wave simulations. For this purpose, one of the main goals was to investigate a basis order selection method based on previous theoretical results. The focus was to determine the relationship between the element size, wave number, accuracy of the solution, and order of the basis functions. In numerical simulations, the parameter choices for a PML [17] and flux splitting were also studied.

This thesis is organized as follows. In Chapter 2, the physical background of acoustic waves in inhomogeneous media is outlined. Starting from linearized conservation laws, the chapter reviews the basic theory of acoustic wave propagation. In Chapter 2, the boundary, initial, and transmission conditions for the acoustic wave equation are discussed.

Chapter 3 describes numerical approximation methods for time-dependent wave problems. For example, a review of the methods used for spatial and time discretizations and for truncating the computational domain are given. The main emphasis is on methods that are used later in this thesis, especially for the PML.

The DG method is discussed in Chapter 4, which outlines the history of the DG method and describes the weak form of the 3D dissipative wave equation. Various choices for flux splitting and basis functions are also discussed.

Chapter 5 is dedicated to computational issues. The chapter begins with a discussion of the parameter choices for the flux splitting scheme. The main emphasis is the study of the effect of non-uniform basis orders on the accuracy of the DG method. In simulations, the effect of the parameter choices for the PML are outlined. This chapter also describes a 3D application experiment, where simulated results are compared with actual measurements. Conclusions are given in Chapter 6.

2 Acoustic field equations

In the field of mechanical wave propagation, two wave types are distinguished depending on the properties of the underlying propagation medium. Traditionally, waves in fluids are called acoustic waves and waves in solids are known as elastic waves. In publication **II**, the elastic wave equation was studied for 2D problems, but the main emphasis was on the acoustic wave equation. Hence, only the derivation of the acoustic wave equation is shown in this thesis. This chapter provides a short introduction to the physical theory of acoustic wave propagation. For a more detailed review of the theory of acoustics, see [18–21]. The derivation given in this thesis follows the derivation provided by Pierce [19].

This chapter gives an introduction to the conservation laws and their linear approximation, which is needed for the short derivation of the linear wave equation. At the end of this chapter, the initial, boundary, and transmission conditions for the acoustic wave equation are outlined.

2.1 CONSERVATION LAWS

The wave equation for acoustic media can be derived starting from two conservation laws. The equation of continuity states that the time-rate of mass moving into a volume through its surface must be equal to the mass increase of the volume. Because this integral law must hold for an arbitrary volume, it can be written in the differential form as follows:

$$\frac{\partial \varrho}{\partial t} + \nabla \cdot (\varrho \boldsymbol{v}) = 0, \tag{2.1}$$

where ϱ is the mass density, t is the time variable, and $\boldsymbol{v}$ is the particle velocity.

The conservation of momentum is a direct consequence of Newton's second law. The acceleration of an arbitrary volume can be expressed as the material derivative, which must be equal to the forces acting on the unit volume. The conservation equation can be written as

$$\varrho \left(\frac{\partial \boldsymbol{v}}{\partial t} + (\boldsymbol{v} \cdot \nabla)\boldsymbol{v} \right) = -\nabla \mathfrak{U}, \tag{2.2}$$

where $\mathfrak{U}$ is the pressure. In Equation (2.2), the term $-\nabla \mathfrak{U}$ stands for the force that is caused by the spatial variation of pressure.

Assuming that changes from the ambient-state values $\boldsymbol{v}_0 = 0$, u_0, and ρ are relatively small, linear approximations for the particle velocity, pressure, and density may be written as

$$\boldsymbol{v}_0 + \boldsymbol{v}(\boldsymbol{x}, t), \quad u_0 + u(\boldsymbol{x}, t), \quad \text{and} \quad \rho(\boldsymbol{x}) + \xi(\boldsymbol{x}, t), \tag{2.3}$$

respectively. Here $\boldsymbol{x} = (x_1, x_2, x_3)$ is the spatial variable. So, the conservation laws reduce to

$$\frac{\partial \xi}{\partial t} + \left\{ \nabla \cdot \rho \boldsymbol{v} + \nabla \cdot \xi \boldsymbol{v} \right\} = 0, \tag{2.4}$$

$$(\rho + \xi) \left(\frac{\partial \boldsymbol{v}}{\partial t} + (\boldsymbol{v} \cdot \nabla) \boldsymbol{v} \right) = -\nabla u. \tag{2.5}$$

The linear approximation, known as the acoustic approximation [19], neglects second- and higher-order terms of conservation laws (2.4) and (2.5). Then, the linear acoustic equations take the form

$$\frac{\partial \xi}{\partial t} = -\left(\rho \nabla \cdot \boldsymbol{v} + \boldsymbol{v} \cdot \nabla \rho \right), \tag{2.6}$$

$$\rho \frac{\partial \boldsymbol{v}}{\partial t} = -\nabla u. \tag{2.7}$$

2.2 ACOUSTIC WAVE EQUATION

The relation between pressure $\mathfrak{U}$ and mass density ϱ is written using a state equation. The state equation is [19]

$$\mathfrak{U} = \mathfrak{U}(\varrho, S_s), \tag{2.8}$$

where S_s is entropy. Pressure is approximated with the first term of the Taylor series expansion of the state equation (2.8) around the equilibrium state (ϱ, S_{s0}) as [19]

$$\mathfrak{U} \approx u_0 + \left(\frac{\partial \mathfrak{U}}{\partial \varrho} \right)_{S_s} \left(\varrho - \rho \right). \tag{2.9}$$

Then, using the assumptions of linearity (2.3), one can write the approximation of the acoustic pressure u as [19]

$$u \approx \left(\frac{\partial \mathfrak{U}}{\partial \varrho} \right)_{S_s} \xi = c^2 \xi, \tag{2.10}$$

where c is the speed of sound.

The chain rule of differentiation applied to the total derivative $\mathcal{D}/\mathcal{D}t$ [19], also known as the full derivative, of pressure $\mathfrak{U}$ gives

$$\frac{\mathcal{D}\mathfrak{U}}{\mathcal{D}t} = \frac{\partial \mathfrak{U}}{\partial \varrho}\frac{\mathcal{D}\varrho}{\mathcal{D}t} = \frac{\partial \mathfrak{U}}{\partial \varrho}\left(\frac{\partial \varrho}{\partial t} + \boldsymbol{\nu}\cdot\nabla\varrho\right). \tag{2.11}$$

With the assumptions of linearity (2.3), acoustic approximation [19], and $\partial\mathfrak{U}/\partial\varrho = c^2$ (see (2.10)), the full derivative of the pressure $\mathfrak{U}$ (2.11) take the form

$$\frac{\mathcal{D}\mathfrak{U}}{\mathcal{D}t} \approx c^2\left(\frac{\partial \xi}{\partial t} + \boldsymbol{\nu}\cdot\nabla\rho\right). \tag{2.12}$$

Substitution of the rearranged linearized conservation law (2.6) to (2.12) gives

$$\frac{\mathcal{D}\mathfrak{U}}{\mathcal{D}t} \approx c^2\left(\frac{\partial \xi}{\partial t} + \boldsymbol{\nu}\cdot\nabla\rho\right) = -c^2\rho\nabla\cdot\boldsymbol{\nu}. \tag{2.13}$$

On the other hand, with the linear approximation [19], the total derivate $\mathcal{D}/\mathcal{D}t$ of the pressure $\mathfrak{U}$ is

$$\frac{\mathcal{D}\mathfrak{U}}{\mathcal{D}t} = \frac{\partial u}{\partial t} + \boldsymbol{\nu}\cdot\nabla u \approx \frac{\partial u}{\partial t}. \tag{2.14}$$

Then, by combining Equations (2.14) and (2.13), the approximation of time derivative of the acoustic pressure u reads

$$\frac{\partial u}{\partial t} = -c^2\rho\nabla\cdot\boldsymbol{\nu}. \tag{2.15}$$

Taking the divergence of (2.7) and differentiating (2.15) with respect to time t, we obtain

$$\nabla\cdot\frac{\partial \boldsymbol{\nu}}{\partial t} = -\nabla\cdot\left(\frac{1}{\rho}\nabla u\right), \tag{2.16}$$

$$\frac{\partial^2 u}{\partial t^2} = -c^2\rho\nabla\cdot\frac{\partial \boldsymbol{\nu}}{\partial t}. \tag{2.17}$$

Therefore, the acoustic wave equation for defining wave propagation and scattering in the heterogeneous media is obtained by substituting (2.16) with (2.17)

$$\frac{1}{\rho c^2}\frac{\partial^2 u}{\partial t^2} = \nabla\cdot\left(\frac{1}{\rho}\nabla u\right). \tag{2.18}$$

2.3 INITIAL, BOUNDARY, AND TRANSMISSION CONDITIONS

For the unique solution of the acoustic wave equation (2.18), initial and boundary conditions are needed. The initial conditions for the acoustic wave equation are

$$u = u_{i1} \quad \text{at} \quad t = 0, \tag{2.19}$$

$$\frac{\partial u}{\partial t} = u_{i2} \quad \text{at} \quad t = 0, \tag{2.20}$$

where u_{i1} and u_{i2} contain the given initial values.

In this study, three boundary conditions for the boundary of domain Ω are considered. These are the Neumann, Dirichlet, and impedance-type boundary conditions. All of these conditions can be expressed using the following formula:

$$\sigma \frac{\partial u}{\partial t} + n \cdot \left(\frac{1}{\rho} \nabla u \right) = Q \left(-\sigma \frac{\partial u}{\partial t} + n \cdot \left(\frac{1}{\rho} \nabla u \right) \right) + \sqrt{2\sigma} g \quad \text{on} \quad \Gamma, \tag{2.21}$$

where n is a spatial outward unit normal, g is a source function, the coupling parameter $0 < \sigma \in \mathbb{R}$, and Γ is the exterior boundary of domain Ω. In Equation (2.21), parameter $Q \in \{-1, 0, 1\}$ with the source function g, defines the boundary condition. The coupling parameter σ is discussed in Section 4.2. The equation form for the boundary conditions is used in Section 4.2, where the weak formulation is discussed.

With $Q = -1$, the inhomogeneous Neumann boundary condition is obtained in the form

$$n \cdot \left(\frac{1}{\rho} \nabla u \right) = \sqrt{\frac{\sigma}{2}} g. \tag{2.22}$$

When the source term $g = 0$, Equation (2.22) reduces to a rigid (sound-hard) boundary. $Q = 1$ leads to the following condition:

$$\frac{\partial u}{\partial t} = \frac{1}{\sqrt{2\sigma}} g, \tag{2.23}$$

which is known as the inhomogeneous Dirichlet boundary condition. The sound-soft boundary condition is obtained when source term $g = 0$ in Equation (2.23). Finally, the impedance-type boundary condition is achieved by setting $Q = 0$. Then, Equation (2.21) reduces to

$$\sigma \frac{\partial u}{\partial t} + n \cdot \left(\frac{1}{\rho} \nabla u \right) = \sqrt{2\sigma} g. \tag{2.24}$$

When $\sigma = 1/c$, $Q = 0$, and the source term $g = 0$, the boundary condition (2.21) reduces to the lowest order Engquist-Majda absorbing boundary condition [8].

Wave problems easily lead to domains consisting of piecewise homogeneous materials. In such cases, the wave equation (3.1) is used in each homogeneous subdomain. At material interfaces, however, a suitable transmission condition must be defined.

Let us consider that the domains Ω^+ and Ω^- are occupied by different but homogeneous acoustic fluids. Hence, the wave fields $u^+ = u|_{\Omega^+}$ and $u^- = u|_{\Omega^-}$ satisfy the acoustic wave equation, respectively. On the adjacent interface of the domains Ω^+ and Ω^-, labeled as Γ^t, two conditions must be satisfied. That is, the acoustic pressures on both sides and, on the other hand, the particle velocities normal to the boundary must be equal. In the equation form, the transmission conditions can be written as

$$\begin{aligned} u^+ &= u^- \\ n^+ \cdot \boldsymbol{v}^+ &= n^- \cdot \boldsymbol{v}^- \end{aligned} \qquad \text{on} \quad \Gamma^t. \tag{2.25}$$

3 Numerical approximation methods

This chapter discusses the standard tools used for approximating hyperbolic partial differential equations (PDEs). Because this thesis focuses on acoustic wave propagation, the acoustic wave equation is written as a first-order linear hyperbolic system. The first-order system is useful because a large number of numerical techniques have been developed for conservation laws characterizing similar first-order PDEs.

Numerical approximation of the time-domain wave problems in heterogeneous media and in general geometries is a challenging task. Analytical solutions can only be derived for the simplest wave problems and the computational complexity of numerical methods increases rapidly with an increase in the wave number. With standard numerical tools, such as the low-order finite difference (FD) [1], the finite volume (FV) [21], and the finite element (FE) [2] methods, the rule of thumb is that approximately 10 discretization points per wavelength are needed to obtain tolerable accuracy [22]. This requirement can lead to extremely large and impractical computational tasks. These approaches suffer from numerical dispersion and dissipation, which force the use of dense spatial discretization and short time steps in the time integration. On the other hand, when the size of the computational domain at a given frequency increases, the density of the spatial discretization must increase to maintain an acceptable error level. This is commonly known as numerical pollution [23–26].

Many problems in acoustics are physically unbounded, which means that the sound field extends from the source to infinity. To evaluate the field numerically, the unbounded problem must be replaced with a bounded domain. The truncation condition is approximated on the exterior boundary of the computational domain using an Engquist-Majda type absorbing boundary condition [8]. Unfortunately, the absorbing boundary condition (in the 2D and 3D problems) affects the accuracy of the solution due to unwanted reflections arising from the boundaries. One promising approach for reducing these reflections is a numerical damping layer called the perfectly matched layer (PML) [9].

In the time-domain problems, one of the most challenging tasks is to choose the most suitable time integration method for approximating the time derivatives. In most cases, implicit approaches are more stable than explicit approaches, but the implicit scheme is computationally more demanding. On the other hand, the length of the time-step plays an important role in the stability and accuracy of the numerical solution. Histori-

cally, several approaches have been proposed to obtain a stable time integration method for approximating the time derivatives. These include the Runge-Kutta [10] (explicit and implicit), Crank-Nicolson [27] (implicit), and arbitrary high-order derivatives time integration approaches using arbitrary high-order derivatives with local time stepping [28].

The remainder of the chapter is organized as follows. In Section 3.1, the 3D acoustic wave equation is written in the form of the first-order linear hyperbolic system. Section 3.2 outlines the classical full-wave methods used for approximating wave propagation. In Section 3.3 the methods used for truncating unbounded problems are outlined.

Time integration methods used for approximating time derivatives are discussed in Section 3.4. Section 3.4 provides an overview of the methods that are commercially used with the discontinuous Galerkin (DG) method [6]. The stability and accuracy of time-stepping is discussed in Section 3.5. The Courant-Friedrichs-Lewy (CFL) number [29, 30] is used to characterize the length of the time step in the time integration cycles during the computation.

3.1 LINEAR HYPERBOLIC SYSTEM

This section outlines the formulation of a 3D dissipative acoustic wave equation as a linear first-order hyperbolic system. In Chapter 2, the acoustic wave equation was derived for non-dissipative media, but here the dissipation term is taken into account. Let Ω be a bounded Lipschitz domain in $\mathbb{R}^3$, $\boldsymbol{x} = (x_1, x_2, x_3) \in \Omega$ is the spatial variable, and $t \in [0, T]$ is time. The acoustic pressure u in the dissipative media satisfies the following equation

$$\frac{1}{\rho c^2}\frac{\partial^2 u}{\partial t^2} + \beta\frac{\partial u}{\partial t} = \nabla \cdot \left(\frac{1}{\rho}\nabla u\right) \quad \text{in} \quad \Omega, \tag{3.1}$$

where ρ is the density, c the speed of sound, t is time, and $\beta \geqslant 0$ is the absorption coefficient. The effect of the absorption coefficient β for the accuracy of the numerical solution was discussed in publication **III** using numerical experiments. Originally, dissipation model $\beta\partial u/\partial t$ was used for dissipative electromagnetic waves [31, 32]. It has since been shown, however, that the attenuation model describes the dispersive attenuation of many soft tissues in acoustic problems [31, 33]. Based on the physical phenomena that cause wave attenuation, different models need to be used (see [20, 32, 34, 35]).

To write the dissipative wave equation (3.1) as a linear hyperbolic sys-

tem, vector $\boldsymbol{u}$ is defined as

$$\boldsymbol{u} = \begin{pmatrix} \boldsymbol{u}_1 \\ \boldsymbol{u}_2 \\ \boldsymbol{u}_3 \\ \boldsymbol{u}_4 \end{pmatrix} = \begin{pmatrix} \frac{\partial u}{\partial t} \\ \frac{1}{\rho}\frac{\partial u}{\partial x_1} \\ \frac{1}{\rho}\frac{\partial u}{\partial x_2} \\ \frac{1}{\rho}\frac{\partial u}{\partial x_3} \end{pmatrix}. \tag{3.2}$$

According to Equation (3.1), the components of $\boldsymbol{u}$ satisfy the following equations (which are actually the conservation law of mass and conservation law of momentum if the term $\beta \boldsymbol{u}_1$ is ignored (see Chapter 2))

$$\frac{1}{c^2\rho}\frac{\partial \boldsymbol{u}_1}{\partial t} + \beta \boldsymbol{u}_1 = \nabla \cdot \begin{pmatrix} \boldsymbol{u}_2 \\ \boldsymbol{u}_3 \\ \boldsymbol{u}_4 \end{pmatrix} \tag{3.3}$$

$$\rho \frac{\partial}{\partial t} \begin{pmatrix} \boldsymbol{u}_2 \\ \boldsymbol{u}_3 \\ \boldsymbol{u}_4 \end{pmatrix} = \nabla \boldsymbol{u}_1. \tag{3.4}$$

Equations (3.3) and (3.4) can be expressed as a single linear hyperbolic system as follows [36]

$$A\frac{\partial \boldsymbol{u}}{\partial t} + \sum_{j=1}^{3} A_j \frac{\partial \boldsymbol{u}}{\partial x_j} + B\boldsymbol{u} = 0 \quad \text{in} \quad \Omega, \tag{3.5}$$

where matrices A and B are defined as

$$A = \begin{pmatrix} \frac{1}{c^2\rho} & 0 & 0 & 0 \\ 0 & \rho & 0 & 0 \\ 0 & 0 & \rho & 0 \\ 0 & 0 & 0 & \rho \end{pmatrix} \quad \text{and} \quad B = \begin{pmatrix} \beta & 0 & 0 & 0 \\ 0 & 0 & 0 & 0 \\ 0 & 0 & 0 & 0 \\ 0 & 0 & 0 & 0 \end{pmatrix}.$$

Furthermore, in system (3.5), matrices A_1, A_2, and A_3 for the spatial derivatives are

$$A_1 = \begin{pmatrix} 0 & -1 & 0 & 0 \\ -1 & 0 & 0 & 0 \\ 0 & 0 & 0 & 0 \\ 0 & 0 & 0 & 0 \end{pmatrix}, A_2 = \begin{pmatrix} 0 & 0 & -1 & 0 \\ 0 & 0 & 0 & 0 \\ -1 & 0 & 0 & 0 \\ 0 & 0 & 0 & 0 \end{pmatrix},$$

and

$$A_3 = \begin{pmatrix} 0 & 0 & 0 & -1 \\ 0 & 0 & 0 & 0 \\ 0 & 0 & 0 & 0 \\ -1 & 0 & 0 & 0 \end{pmatrix}.$$

3.2 A SHORT REVIEW OF CLASSICAL NUMERICAL METHODS

This section outlines the standard methods used for approximating hyperbolic PDEs. The classical full-wave methods include the FD method, FV method, and FE method. When using the FD, FV, and FE methods, discrete presentations of the spatial derivatives are derived. In the following three sections, these methods are first briefly outlined and the main advantages and disadvantages of each method are discussed. The discussion provided here is based on the introduction written by Hesthaven and Warburton in [7].

There are several other approaches for approximating the propagation of mechanical waves. These include the commonly used ray-tracing technique [37–39] and the boundary element method [40–42].

Finite difference method

The FD method is a traditional and widely used method of numerically approximating different problems of mathematical sciences. Briefly, the idea of the FD method is to first divide the computational domain into a set of structured grid points. Then, a numerical difference approximation is constructed for each grid point of the computational mesh. Similarly, the time derivatives can be approximated using a difference scheme.

One of the original references to the FD method is the work done by Yee [1]. During the last several decades, the FD method has been extensively analyzed and extended to a wide range of applications, including geoacoustic scattering from the seafloor [43], electromagnetic wave scattering [44], and acoustic and elastic wave propagation [45]. FD methods and their dispersive properties have been well described by Cohen [2] and Quarteroni *et al.* [27].

With the FD method, the discretization of general initial-boundary value problems is intuitively simple, which makes the approach very popular. The huge disadvantage of the FD method, however, is that the approach is highly ill-suited to deal with complex geometries. On the other hand, the rule of thumb (10 discretization points per wavelength) forces

the use of dense grids, which can easily lead to impractical computational tasks. Despite the disadvantages of the FD method, it is still heavily investigated, especially in the field of therapeutic ultrasound [4, 46, 47] and propagation of electromagnetic waves [3].

Finite volume method

The FV method is closely related to the FD method, but it has several advantages. It is more flexible for handling computations for complex geometries. In the FV is a method, the solution is computed locally on each cell of the computational mesh and the flow between the adjacent cells is handled using a numerical flux. The FV method does not require a structured mesh (although a structured mesh can also be used). The FV method is especially powerful for coarse non-uniform grids and in calculations where the mesh moves to track interfaces or shocks.

There are several good books in which the FV method is extensively discussed. These books include the book written by Leveque, in which hyperbolic problems are considered [21], and the book written by Versteeg and Malalasekra [48] that deals with computational fluid dynamics. For FV methods, we refer to Piperno [49], in which the time-dependent Maxwell's equations are approximated in 2D problems. Similarly, electromagnetics is studied using the FV method by Cioni *et al.* in [50]. Solutions of the non-linear, steady-state diffusion equation are given by Moroney and Turner [51].

Finite element method

The FE method is considered to be the gold standard for numerically approximating wave propagation. The idea behind the FE method is to write the weak form for the studied IBV problem. Formally, the procedure is to multiply the system with the test functions and then integrate the obtained system over the domain Ω. Then, the classical Galerkin scheme is obtained by approximating the test functions and the physical parameter (or parameters) of the IBV problem with the same basis functions. For more details of weak form derivation using the FE method, see [2].

The FE method is used by approximating continuous quantities as a set of elements, often regularly spaced into a computational mesh. The FE method can be adapted to problems of complex geometry. This feature makes the FE method an extremely powerful tool in several fields of physics and engineering, including heat transfer, fluid mechanics, and mechanical systems.

A huge improvement in the FE method is the use of mass lumping, which is discussed in references [2, 52, 53]. In this approach, the mass matrix is diagonal. A diagonal mass matrix leads to significant computational advantages for calculations that involve the inverse of this matrix. To read more extensive reviews and recent studies related to the FE method, see [2, 5, 54–56] for Maxwell's equations, [57] for solid mechanics, [25] for the time-harmonic wave equation, and [58] for compressible Euler equations. A good review paper of the FE method used for the time-harmonic acoustics is given by Thompson [59].

In this thesis the FE method was used (see publication **I**) for approximating the time-dependent acoustic wave equation in 2D problems. In publication **I**, the solutions obtained using the DG method and the FE method with linear and quadratic bases were compared.

3.3 ABSORBING BOUNDARY CONDITIONS

Unfortunately, in the case of unbounded problems, the absorbing boundary condition (Equation (2.24) with $\sigma = 1/c$ and $g = 0$) affects the accuracy of the solution, because unphysical reflections arise from the boundary. Numerous methods have been proposed to reduce the unwanted numerical reflections, e.g., the arbitrarily high-order absorbing boundary condition (AHOC) published by Collino [60]. The 3D version of the AHOC boundary condition was subsequently given by Grote and Keller [61, 62]. The AHOC method was studied in detail by Givoli [63, 64].

The PML is another promising solution for reducing spurious reflections. The idea behind the PML is to construct a numerical damping layer that attenuates the amplitude of the wave without reflections. The PML was first used for Maxwell's equations by Bérenger [9]. There are several formulations of the PML. These include the original version in which the physical variables are split according to the terms of the spatial derivative. Another choice is to use the unsplit version of the PML, which was studied by Hu [17]. The Euler equations with a mean flow in the 2D problems are investigated [17]. Generally, the PML is a widely used and analyzed approach, see [2, 65–69].

Perfectly matched layer for three-dimensional wave equation

The initial step in the derivation of the unsplit version of the PML is to transform the system to the frequency-domain by replacing the time

derivative operator by

$$\frac{\partial}{\partial t} = -i\omega,$$

where i is the imaginary unit and ω denotes the angular frequency. We then introduce the complex stretched [66,70] differential operator for the spatial terms as

$$\frac{\partial}{\partial x_j} \rightarrow \frac{\partial}{\partial x_j'} = \left(\frac{1}{1 + \frac{id_{x_j}}{\omega}} \right) \frac{\partial}{\partial x_j}, \quad j = 1, \ldots, 3, \tag{3.6}$$

where $0 \leqslant d_{x_j}(\boldsymbol{x}),\ j = 1, \ldots, 3$ (defined later in this section, in Equation (3.11)). Then, the frequency-domain system is multiplied by the term

$$\prod_{j=1}^{3} \left(1 + \frac{id_{x_j}}{\omega} \right). \tag{3.7}$$

After multiplying the frequency-domain system with the term (3.7), the system can be transformed back to the time-domain [17].

With the steps defined in the previous and the auxiliary variables $\boldsymbol{q}_1, \boldsymbol{q}_2$, and $\boldsymbol{q}_3$, the unsplit version of the PML for system (3.5) is

$$A\frac{\partial \boldsymbol{u}}{\partial t} + \sum_{j=1}^{3} A_j \frac{\partial \boldsymbol{u}}{\partial x_j} + B\boldsymbol{u} + G\left(\boldsymbol{q}, \boldsymbol{u}\right) = 0, \tag{3.8}$$

$$\frac{\partial \boldsymbol{q}_1}{\partial t} = \boldsymbol{u}, \frac{\partial \boldsymbol{q}_2}{\partial t} = \boldsymbol{q}_1, \frac{\partial \boldsymbol{q}_3}{\partial t} = \boldsymbol{q}_2, \tag{3.9}$$

where

$$\begin{aligned} G\left(\boldsymbol{q}, \boldsymbol{u}\right) \quad = \quad & \left(d_{x_2} + d_{x_3}\right) A_1 \frac{\partial \boldsymbol{q}_1}{\partial x_1} + \left(d_{x_1} + d_{x_3}\right) A_2 \frac{\partial \boldsymbol{q}_1}{\partial x_2} \\ & + \left(d_{x_1} + d_{x_2}\right) A_3 \frac{\partial \boldsymbol{q}_1}{\partial x_3} + d_{x_2} d_{x_3} A_1 \frac{\partial \boldsymbol{q}_2}{\partial x_1} \\ & + d_{x_1} d_{x_3} A_2 \frac{\partial \boldsymbol{q}_2}{\partial x_2} + d_{x_1} d_{x_2} A_3 \frac{\partial \boldsymbol{q}_2}{\partial x_3} + \left(d_{x_1} + d_{x_2} + d_{x_3}\right) A\boldsymbol{u} \\ & + \left(d_{x_1} d_{x_2} + d_{x_1} d_{x_3} + d_{x_2} d_{x_3}\right) A\boldsymbol{q}_1 + d_{x_1} d_{x_2} d_{x_3} A\boldsymbol{q}_2 \\ & + \left(d_{x_1} + d_{x_2} + d_{x_3}\right) B\boldsymbol{q}_1 + \left(d_{x_1} d_{x_2} + d_{x_1} d_{x_3} + d_{x_2} d_{x_3}\right) B\boldsymbol{q}_2 \\ & + d_{x_1} d_{x_2} d_{x_3} B\boldsymbol{q}_3. \end{aligned} \tag{3.10}$$

For simplicity, in Chapter 4, we use the term G in equations shown in the weak formulation of the DG scheme. Note, however, that the term

G is only required in the PML domain. Nevertheless, to simplify the discussion we do not distinguish between PML and non-PML ($G = 0$) regions.

The damping coefficients are defined as

$$d_{x_\ell}(\boldsymbol{x}) = d_0 \left| \frac{x_\ell - x_0}{\vartheta} \right|^\eta, \quad \ell = 1, \ldots, 3, \tag{3.11}$$

where $0 \leqslant d_0 \in \mathbb{R}$ is the parameter for PML, x_0 denotes the spatial position from which the numerical damping starts, ϑ is the PML thickness, and parameter η is the power for the PML. The effect of these parameters is simulated in publication **III** and Chapter 5 (in Section 5.1.3).

3.4 OVERVIEW OF TIME INTEGRATION METHODS

The approximation of the time derivatives of the studied initial-boundary value problem poses a challenging task. Some of the time-stepping schemes used with the DG method are outlined below.

The most traditional time integration method used with the DG is the explicit Runge-Kutta (RK) approach [10, 71]. The RK approach for the DG method was originally published by Cockburn and Shu [10] and [71]. Subsequently, the RK approach, and its extensions, such as explicit low-storage Runge-Kutta (LSRK) and the fourth-order explicit, singly diagonally implicit Runge-Kutta (ESDIRK4), has been widely studied in several fields of physics [11–13, 72–74]. The implicit Crank-Nicolson (CN) implementation with the DG method was investigated in [75]. In [75], Maxwell's equations are approximated in 2D problems. Another possible implementation also uses the Newmark method, which is examined in [14] for approximating wave propagation. The RK, LSRK, ESDIRK4, and CN methods were also examined in our previous papers **I**-**IV**.

A time integration method that has been increasingly popular in conjunction with the DG method is the ADER time integration approach using arbitrary high-order derivatives. In the ADER time integration method, the main idea is a Taylor expansion in time in which time derivatives are replaced by spatial derivatives. The ADER schemes were originally published in [15, 16] and studied further in [76, 77]. Recently, the ADER scheme with the DG method was successfully applied to solve the elastic wave equation [28, 78–81].

A possible approach to improve the time integration method is to use local time-stepping (LTS) schemes. The idea behind the LTS schemes is that the length of the time step is selected individually for each element

of the computational mesh. In this manner, the time needed for computations can be decreased and the CFL number (see Equation (3.12)) is optimal for every element of the mesh. Benefits of the LTS schemes will be more highly realized in the highly non-uniform meshes, because the mesh parameter is totally different for each element. The disadvantage of the LTS schemes is that efficient parallelization of the solver code is complicated [82]. Despite the disadvantages, the LTS schemes are widely studied and developed [28,77,83–85].

An approach that is actively used with the DG method is the space-time DG method. This approach uses basis functions for the spatial and time derivatives. The space-time method was originally published by Richter [86] and by Lowrie *et al.* [87]. The space-time DG method was studied for the nonlinear Schrödinger equation [88], for the acoustic wave equation [89], and for elastodynamic problems [90]. Detailed discussion of the space-time DG method can be found in [91].

3.5 COURANT-FRIEDRICHS-LEWY NUMBER

During the time integration cycles, the length of the time step needs to be defined. The length of the time step can be determined using the CFL number. The concept of the CFL number was originally published in German in 1928 [29] and republished in English [30]. In [29], the aim was to prove the existence of solutions of certain PDEs. Consequently, while proving the existence, Courant, Friedrichs, and Lewy found the necessary condition to stabilize the numerical methods. For more detailed discussion of the CFL number, see [21].

In the equation form, the CFL number is

$$\mathrm{CFL} = \frac{\delta_t c}{h_{\min}}, \tag{3.12}$$

where δ_t is the length of the time step, c is the speed of sound, and $h_{\min}$ is the smallest distance between two vertices in the computational mesh. The mesh parameter $h_{\min}$ can be either the global minimum of the elements of the mesh or the local value for each element. There are several limits for the CFL number in terms of obtaining a stable solution. For example, these limitations in cases using the finite element or finite difference methods are examined in [2].

Because we are focusing on DG schemes, we discuss the limits for the CFL number when the DG method is used with the RK time integration approach. In the case of the RK method, the stability limit for the CFL

number is

$$\mathrm{CFL} < \frac{1}{2p+1}, \tag{3.13}$$

where p is the polynomial order of the basis functions. The condition of Equation (3.13) has been proven for the polynomial order $p = 1$ [10]. There is no analytical proof for higher order polynomials [92]. In practice, the stability limit predicts that when the order of the basis functions is increased, the length of the time step decreases, which increases the computation time needed to approximate the time derivatives of the studied IBV problem and is a huge drawback of the high-order DG schemes. For more detailed discussion of the CFL number with DG methods, see [7] and references therein.

4 Discontinuous Galerkin method

The discontinuous Galerkin (DG) method was originally introduced by Reed and Hill [6]. The idea of the DG method is to decompose the original problem into a set of subproblems that are connected using an appropriate transmission condition (known as the numerical flux). For geometric partitioning of the computational domain, the DG method uses standard disjoint finite element meshes. In the DG method, each element of the computational mesh determines a single subproblem. By setting the material properties for each subproblem to be constant, the solution is calculated separately for each element of the computational mesh. The solution for the whole computational domain is achieved by summing over all the elements of the mesh.

This chapter provides a brief history of the DG method. In Section 4.1, some applications that have been actively researched for the DG scheme are reviewed. In this chapter, a weak formulation of the first-order hyperbolic system of Chapter 3 is given. Different choices for the type of basis function used with the DG methods are also discussed. The types of basis functions considered in Section 4.3 are limited to the polynomial and plane wave basis. The chapter ends with a discussion of the theoretical background (error estimates) of the DG method.

4.1 A BRIEF HISTORY OF DISCONTINUOUS GALERKIN METHOD

This section provides a short introduction to the history of the DG method. A more extensive overview is given in several references, including the book written by Hesthaven and Warburton [7], the collection of articles edited by Cockburn *et al.* [90], and the review article written by Xu and Shu [93].

In 1973, Reed and Hill [6] first applied the DG method to approximate the steady-state neutron transport equation. The DG method was subsequently extended to numerous fields of physics and engineering. The popularity of this method has increased since the early 1990s. Some of these applications are briefly outlined below.

One of the traditional research topics is in electromagnetism (Maxwell's equations) [94–97]. Historically, numerical approximation of Maxwell's equations in the time-domain has been a challenging. Particularly for realistic 3D cases, the electromagnetic problems can easily lead to im-

practical computational tasks. In engineering physics, however, modeling of Maxwell's equations plays an important role, with applications ranging from the modeling of wave scattering from airplane surfaces [90] to the modeling of wave propagation in the ground (ground-penetrating radar) [98].

Another extension is the study of wave propagation in an elastic medium (the elastic wave equations), which was extensively studied by Käser *et al.* [78, 81], Dumbser *et al.* [28, 79], and de la Puente *et al.* [80]. In [28,78–81] the DG method is used with the arbitrary high-order derivatives time integration approach using arbitrary high-order derivatives (see Section 3.4). In these references, several phenomena are discussed in the field of elastic waves for 2D and 3D problems, including viscoelastic attenuation of the wave and wave propagation in isotropic and anisotropic media. On the other hand, *p*-adaptivity and local time stepping of the solver have also been described [28]. Recently, the arbitrary high-order derivatives scheme was also extended to coupled problems (acoustic and elastic wave equations) [99]. The DG method has been evaluated in several studies, including the modeling of shallow water equations [100–102], compressible and incompressible Navier-Stokes equations [103–105], and plasma physics [106, 107].

Recently, Klöckner *et al.* extended the DG method to run on graphics processing units to approximate the time-dependent Maxwell's equation in realistic 3D problems [108]. The results reported in [108] predict that computation time is largely decreased when the DG method is computed on a graphics processing unit.

4.2 WEAK FORMULATION

This section outlines the weak form of the DG method for the first-order hyperbolic system shown in Equation (3.5). The derivation shown here is based on Monk and Richter [89] and Falk and Richter [109].

For the weak formulation, the domain Ω is divided into N elements (in this thesis, the tetrahedral elements in 3D and triangular elements in 2D are used) so that

$$\Omega = \bigcup_{\ell=1}^{N} \Omega_\ell.$$

In the following, the boundary of the arbitrary element Ω_ℓ is denoted by $\Gamma(\Omega_\ell)$.

As a summary, we show only the final weak form. The weak form is obtained by first multiplying the system with the test function and in-

tegrating over an arbitrary element. Then, by integrating the parts, the integral over the surface is obtained. The flux splitting method is used for the surface integral term. Then, by integrating parts again and finally summing over all the elements of the computational mesh, the weak form is obtained. Therefore, if $\boldsymbol{u}_\ell$ denotes the field in the element Ω_ℓ, $\ell = 1, \ldots, N$ and $\boldsymbol{v}_\ell$ is the corresponding test function, the entire weak form is obtained by summing over all of the elements

$$\begin{aligned} & \sum_{\ell=1}^{N} \left[\int_{\Omega_\ell} \boldsymbol{v}_\ell^\top \left(A \frac{\partial \boldsymbol{u}_\ell}{\partial t} + \sum_{j=1}^{3} A_j \frac{\partial \boldsymbol{u}_\ell}{\partial x_j} + B\boldsymbol{u}_\ell + G_\ell \right) dV \right. \\ & \left. + \sum_{m=1}^{N} \int_{\Gamma_i(\Omega_\ell)} \boldsymbol{v}_\ell^\top D^- (\boldsymbol{u}_m - \boldsymbol{u}_\ell)\, dA - \int_{\Gamma_e(\Omega_\ell)} \boldsymbol{v}_\ell^\top \left(D - \mathcal{N}\right) \boldsymbol{u}_\ell \, dA \right] \\ = \; & - \sum_{\ell=1}^{N} \int_{\Gamma_e(\Omega_\ell)} \boldsymbol{v}_\ell^\top \boldsymbol{g} \, dA, \end{aligned} \tag{4.1}$$

where matrices A, A_1, A_2, A_3, and B were introduced in Section 3.1 and function G is shown in Equation (3.10). All other parameters are defined later in this section. Note that in the weak form (4.1) the summation term over the neighboring elements (denoted by the subscript m) exists only if the elements Ω_ℓ and Ω_m share a common interface so that $\Gamma_i(\Omega_\ell) \cap \Gamma_i(\Omega_m) \neq \varnothing$.

Because the weak form of the DG method is written elementwise (4.1), the numerical flux between adjacent elements must be defined. For this purpose, we define a boundary matrix D

$$D = \sum_{j=1}^{3} n_j A_j, \quad n = (n_1, n_2, n_3), \tag{4.2}$$

where n is a spatial outward unit normal. The boundary matrix D is then decomposed into its components; that is, the "inflow boundary" D^- and "outflow boundary" D^+ flux matrices [89], using its eigenvectors and eigenvalues.

The choice of flux splitting affects the stability and accuracy of the DG method [110]. A commonly used flux splitting method is the Lax-Friedrichs method, which was previously investigated in [95]. Another method used for flux splitting is the Harten-Lax-van Leer approach [111]. Harten-Lax-van Leer flux is discussed in Leveque [21] and Qie *et al.* [112]. In Qie *et al.* [112] a comparison study of numerical fluxes with the Euler equation is given. A similar comparison for the diffusion problems was performed in [113]. For a detailed discussion of flux splitting methods,

see [7] and references therein.

In this thesis, we used the approach in which the numerical flux between inner elements is dealt with using an impedance-type boundary condition. To write the boundary conditions (the numerical fluxes) for the common interface of two adjacent elements and for the exterior boundary, a new matrix must be defined. For this purpose, coupling matrix S is defined

$$S = \begin{pmatrix} \sigma & 0 & 0 & 0 \\ 0 & 1 & 0 & 0 \\ 0 & 0 & 1 & 0 \\ 0 & 0 & 0 & 1 \end{pmatrix},$$

where parameter $0 < \sigma \in \mathbb{R}$. Because the choice of σ affects the accuracy of the approximation, our choice is based on the results shown in **I** and in Chapter 5 (in Section 5.1.1). Based on the results, the practical choice for σ is

$$\sigma = \frac{2}{c^+ + c^-},$$

where c^+ and c^- are the wave speeds of the elements that share a common interface.

Using the definition of matrix S, the boundary matrix D can be written in a more general form as follows

$$D = \frac{1}{\sigma} SDS,$$

then, by using the "outflow" and "inflow" boundary flux matrices

$$D = \frac{1}{\sigma} SD^+S + \frac{1}{\sigma} SD^-S.$$

Next, using the eigenvectors and eigenvalues of boundary matrix D, the matrices D_σ^+ and D_σ^- are written in the following form

$$\begin{aligned} D_\sigma^+ &= \frac{1}{2\sigma} \begin{pmatrix} -\sigma \\ n_1 \\ n_2 \\ n_3 \end{pmatrix} (-\sigma, n_1, n_2, n_3), \\ D_\sigma^- &= -\frac{1}{2\sigma} \begin{pmatrix} \sigma \\ n_1 \\ n_2 \\ n_3 \end{pmatrix} (\sigma, n_1, n_2, n_3). \end{aligned}$$

To rewrite matrices D_σ^+ and D_σ^- in a more compact form, let column vectors $\boldsymbol{l}^+$ and $\boldsymbol{l}^-$ be defined as

$$\boldsymbol{l}^+ = \frac{1}{\sqrt{2\sigma}}(-\sigma, n_1, n_2, n_3), \quad \boldsymbol{l}^- = \frac{1}{\sqrt{2\sigma}}(\sigma, n_1, n_2, n_3).$$

Using the vectors $\boldsymbol{l}^+$ and $\boldsymbol{l}^-$, matrices D_σ^+ and D_σ^- can be decomposed as

$$\begin{aligned} D_\sigma^+ &= (\boldsymbol{l}^+)^\top \boldsymbol{l}^+, \\ D_\sigma^- &= -(\boldsymbol{l}^-)^\top \boldsymbol{l}^-. \end{aligned}$$

On the exterior boundary Γ, the boundary condition (see Equation (2.21)) is

$$(D - \mathcal{N})\,\boldsymbol{u} = \boldsymbol{g} \quad \text{on} \quad \Gamma, \tag{4.3}$$

where matrix D is shown in Equation (4.2), and matrix $\mathcal{N}$ will be defined later in this Section (see Equation (4.5)). The exterior boundary condition (4.3) can be rewritten using the definitions of $\boldsymbol{u}$ and vectors $\boldsymbol{l}^-$ and $\boldsymbol{l}^+$ as follows,

$$\boldsymbol{l}^-\boldsymbol{u} = Q\boldsymbol{l}^+\boldsymbol{u} + g. \tag{4.4}$$

Multiplying Equation (4.4) with the vector $(\boldsymbol{l}^-)^\top$ gives the following equation

$$(\boldsymbol{l}^-)^\top \boldsymbol{l}^-\boldsymbol{u} = Q(\boldsymbol{l}^-)^\top \boldsymbol{l}^+\boldsymbol{u} + (\boldsymbol{l}^-)^\top g.$$

The practical choice for matrix $\mathcal{N}$ is [89]

$$\mathcal{N} = D - 2(D_\sigma^- + Q(\boldsymbol{l}^-)^\top \boldsymbol{l}^+). \tag{4.5}$$

Rearranging the terms in Equation (4.5), the following form is obtained

$$(D - \mathcal{N})\boldsymbol{u} = 2\left(D_\sigma^- + Q(\boldsymbol{l}^-)^\top \boldsymbol{l}^+\right)\boldsymbol{u} = -2(\boldsymbol{l}^-)^\top g. \tag{4.6}$$

The right-hand side of Equation (4.3) is

$$\boldsymbol{g} = -2\left(\boldsymbol{l}^-\right)^\top g. \tag{4.7}$$

4.3 BASIS FUNCTIONS

In this thesis, Legendre polynomials, which are a member of the Jacobi polynomials, are used as basis functions. The Legendre polynomials are discussed in several references, for example, see [27,114]. The polynomial interpolation nodes in a triangle are discussed in references [115, 116].

Similarly, the interpolation points in the tetrahedra are considered in a paper written by Hesthaven and Teng [117] and in the article written by Chen and Babuška [118]. Generally, different basis expansions are compared in [114] and the results predict that the Legendre polynomials produce the smallest condition number for the mass matrix. Because we use relatively high-order basis functions, the low condition number is essential to guarantee a stable solution. Hence, we used the Legendre polynomials in the simulations of this study. In general, the use of Legendre polynomials as the basis functions is a common choice for the DG method, see references [7, 90] and references therein.

Another choice for the type of basis function is to use plane waves instead of the polynomial basis with the DG method [119–121]. These studies are for time-harmonic problems. One reason for using plane waves as the basis is that high-order polynomials are a problematic way to represent highly oscillatory pressure fields. For example, Gabard [120] shows that when using the plane wave basis with the DG method for linearized Euler equations, the system reduces to the ultra-weak variational formulation (UWVF) for the Helmholtz equation as presented in [122]. The connection between the UWVF and the DG method is also shown in [123], in which Maxwell's equations were examined.

The UWVF was originally published by Després and Cessenat [124–126]. The UWVF method contains several similar advantages as the DG method when compared to the traditional approaches, such as the finite element and finite difference methods. For example, the time needed for computations and, consequently, the computational load can be dramatically reduced. Motivated by these advantages, the UWVF method has been significantly developed by Huttunen *et al.* for Helmholtz problems [122, 127], elasticity [128, 129], and electromagnetism [123].

4.4 ERROR ESTIMATES

The first error analysis of the DG method was given by LeSaint and Raviart [130], with two main results; $\mathcal{O}(h^p)$-convergence on a general triangulated mesh and optimal convergence rate $\mathcal{O}(h^{p+1})$ on a cartesian mesh of cell size h and polynomial order p. The next major analysis of DG methods was given by Johnson and Pitkäranta [131]. They improved the results reported in [130], showing $\mathcal{O}(h^{p+1/2})$-convergence on general meshes. In 1988, Richter [132] reported the optimal rate of convergence of $\mathcal{O}(h^{p+1})$ for a semi-uniform triangulation. All of these studies are given to linear equations. There have also been several studies of non-linear scalar hyperbolic systems, see [133–136].

There have been relatively fewer reports regarding the issue of wave propagation of the DG method. Johnson and Pitkäranta [131] performed a Fourier analysis of the DG method for the case of $p = 1$. Hu *et al.* [137] studied numerical dissipation and dispersion errors of the DG method for 1D and 2D wave equations.

The polynomial order selection method is one of the major research topics of this thesis. The proposed method is highly based on, and motivated by, the results derived by Ainsworth and his collaborators [138]. In [138] the dispersive and dissipative properties of the high-order DG scheme for the transport equation are given. Furthermore, Ainsworth *et al.* [139] considered the dispersive and dissipative properties for second-order wave equations. The proposed basis order selection method is discussed in publications **II** and **III** and Chapter 5 (in Section 5.1.2).

5 Computational issues

In this chapter, we discuss the practical aspects of the numerical implementation of the discontinuous Galerkin (DG) method for time-domain wave problems and outline the numerical results of publications **I-IV**.

This chapter is divided into two main parts. In the first part, the numerical background of the application example shown in this thesis is described, beginning with a discussion of the computational procedure, which contains more specific information about the DG solver written during the thesis project. Section 5.1 also contains a discussion of the effect of several parameters that strongly affect the accuracy of the solution obtained using the DG method. In the following sections, the effect of the flux coupling parameter, a method for choosing the degree of the polynomial basis functions and the influence of the perfectly matched layer (PML) parameters are studied.

In the second part of the chapter, the feasibility of the DG method in practice is discussed. For this purpose, a 3D experiment for the acoustic wave equation is computed. In particular, in the given example, sound is generated using a tweeter element of a real loudspeaker. In this case, acoustic scattering is studied from an infinitely long cylinder-shaped object. In the model problem, the numerical results are compared to the actual measurements.

5.1 COMPUTATIONAL IMPLEMENTATION

The DG solver used in this thesis was written using the C/C++ programming language. Furthermore, the message passing interface was used to parallelize the program for 3D problems. The idea behind an efficient parallelized DG solver code is that the computational mesh is partitioned into n_p parts, where n_p is the number of processors. After the partitioning, each processor computes only the part of the matrices needed for computations. In the current work, mesh partitioning was performed using Metis software [140]. The load balancing was evaluated after mesh partitioning because the polynomial basis order was not constant for all elements of the mesh. In this thesis, computational meshes were constructed using the Gambit® or the Femlab/Comsol Multiphysics® platforms. Several published articles have outlined parallelization strategies, see [83, 141–144]. The solver code written during this project was highly influenced by these references.

Some of the computations used for this doctoral thesis project were performed using a PC cluster containing 24 2.6 GHz Pentium 4 processors and 96 GB total RAM. We also used a Cray XT4/XT5 massively parallel processor supercomputer Louhi, which is a part of the IT Center for Science (CSC) computing environment.

5.1.1 Flux coupling parameter

In publication **I**, the effect of the flux coupling parameter σ on the accuracy of the numerical solution was studied. Wave propagation was studied in the homogeneous domain $\Omega \in \mathbb{R}^2$ so that $\Omega = [-1,\ 1]^2$. The PML was not used in this case. The normalized material parameters for the wave equation (Equation (3.1)) were chosen so that the speed of sound $c = 2$, density $\rho = 1$, and attenuation coefficient $\beta = 0$. The initial condition, for the system (3.5), was $\boldsymbol{u}(t = 0) = 0$.

On the exterior boundary Γ of domain Ω, an impedance-type boundary condition (2.21) with $Q = 0$ and $\sigma = 1/c$ was used. The source function g for Equation (2.24) was defined in Equation (5.2). Time integration was performed using the Crank-Nicolson method. Furthermore, the time span was $t \in [0,\ 1]$, which means that during the simulation the wave propagated from the left boundary $x_1 = -1$ to the right boundary $x_1 = 1$.

The analytic solution for this model problem is

$$\boldsymbol{u} = \begin{pmatrix} g(ct - \boldsymbol{k}\cdot\boldsymbol{x}) \\ -\boldsymbol{k}_1 g(ct - \boldsymbol{k}\cdot\boldsymbol{x}) \\ -\boldsymbol{k}_2 g(ct - \boldsymbol{k}\cdot\boldsymbol{x}) \end{pmatrix}, \tag{5.1}$$

where vector $\boldsymbol{k} = (\boldsymbol{k}_1, \boldsymbol{k}_2) = (1, 0)$,

$$g(s) = \begin{cases} 1 - \cos(\omega(s-1)) & \text{if } 0 \leq \frac{\omega}{2\pi}(s-1) \leq 1/2 \\ 0 & \text{otherwise.} \end{cases}, \tag{5.2}$$

where $\omega = 4\pi$ is the angular frequency.

The analytic and numerical solutions were compared at the final time instant if the whole computational domain Ω or in one spatial position as a function of time using the discrete L_2-error. The error was computed using

$$\sqrt{\frac{\sum_\ell \left(u_n(t_\ell) - u_e(t_\ell)\right)^2}{\sum_\ell \left(u_e(t_\ell)\right)^2}}, \tag{5.3}$$

where u_n is the numerical solution and u_e is the analytic solution. The

relative error (Equation (5.3)) was computed only for component u_1 in all experiments described in this thesis.

On all element faces on the exterior boundary of the domain, the value for parameter σ was fixed ($\sigma = 1/c = 0.5$ in all cases). The value of parameter σ on the exterior boundaries comes from the definition of the physical absorbing boundary condition (ABC) (see Equation (2.24)). Figure 5.1 shows the relative error as a function of the parameter σ used on the interior element interfaces. The relative error was computed as a function of time at the spatial position $(x_1, x_2) = (0.5, 0)$. Table 5.1 shows details of the computational meshes used in these studies. The value for the Courant-Friedrichs-Lewy (CFL) number (see Equation (3.12)) was small enough to ensure that the error arising from time integration does not dominate the relative error (CFL $= 0.05$). The results predict that the optimal choice for the inter-element coupling parameter σ was 0.5, which corresponded to the case $\sigma = 1/c$.

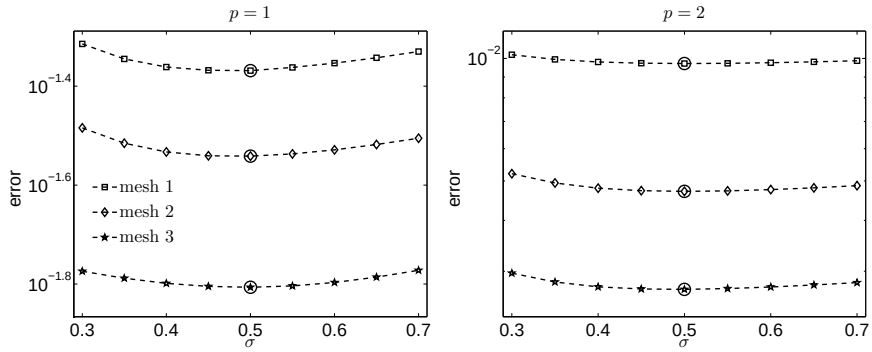

Figure 5.1: The relative error as a function of the coupling parameter σ for two polynomial basis orders ($p = 1$ (left) and $p = 2$ (right)) in meshes (1,2,3). The CFL number was 0.05 and the circles denote the point where the minimum relative error was obtained.

Table 5.1: The number of triangle elements and vertices in computational meshes used in the computations, $h_{\min}$ denotes the shortest distance between two vertices in the mesh, and $h_{\max}$ denotes the longest distance between two vertices in the mesh.

	mesh 1	mesh 2	mesh 3
elements	1724	2426	3264
vertices	909	1268	1695
$h_{\min}$	0.039	0.033	0.025
$h_{\max}$	0.115	0.094	0.087

5.1.2 Non-uniform basis order

During this thesis project, we focused on controlling the basis degree for an arbitrarily-sized element instead of refining the mesh size (commonly known as p-adaptivity). Several studies discuss p- and h-adaptive DG methods [28, 91, 145–147].

To construct a relationship between the element size, order of the basis functions, accuracy of the solution, and wave number, results given by Ainsworth [138] were studied. In [138], a super-exponential rate of convergence was derived when

$$2p + 1 > kh + \mathcal{O}\left(hk\right)^{1/3}, \tag{5.4}$$

where p is the order of the basis function, k is the wave number, h is the element size parameter, and $\mathcal{O}$ denotes the error function. The theoretical results indicate that the practical way to choose the degree of the basis functions for an arbitrary element is to set [138]

$$2p + 1 \approx \kappa kh, \tag{5.5}$$

where $1 < \kappa \in \mathbb{R}$ is a free parameter. The free parameter κ is not, however, useful in practice. The motivation behind the basis order selection method provided in this thesis was to determine the dependence between the relative error and the free parameter κ.

Two-dimensional case

In a 2D case, wave propagation was studied in a homogeneous medium without using the PML. The computational domain for this experiment was a square, so that $\Omega = [-1,\ 1]^2$. The normalized material parameters for the wave equation (3.1) were chosen so that the wave speed $c = 1$, density $\rho = 1$, and absorption coefficient $\beta = 0$. The initial condition $\boldsymbol{u}(t = 0) = 0$ in this model problem. On the exterior boundary Γ of the domain Ω, an impedance-type boundary condition (2.21) with $Q = 0$ and $\sigma = 1/c$ was evaluated. The exact solution for this experiment is the same as that used in Section 5.1.1 (Equation (5.1)).

The source function g for Equation (2.24) is defined as (known as the Mexican hat or Ricker wavelet)

$$g(s) = a_1 \left(0.5 + a_2 \left(s - t_0\right)^2\right) \exp\left(a_2 \left(s - t_0\right)^2\right) \quad \forall s \geqslant 1, \tag{5.6}$$

where a_1 and t_0 are free parameters and $a_2 = -\left(\pi f\right)^2$ (f is the frequency).

In this experiment, frequency $f = 2$, parameter $a_1 = -1$, and $t_0 = 0.75$.

In this experiment (and also in the 3D case), wave propagation was studied in regularly refined meshes. Our aim was to find equations to approximate orders for the basis functions that give a relatively constant error level. For this purpose, we plotted the polynomial order p as a function of the parameter hk for three levels of the relative error. The stipulated error levels were 10, 1, and 0.1%. For these results, we applied data fitting the form

$$p = ahk + b = \frac{2\pi ah}{\lambda} + b, \tag{5.7}$$

where p is the polynomial order, h is the mesh parameter, k is the wave number, and λ is the wavelength. In this 2D problem, mesh parameter h was the largest distance between the two vertices in the element of the computational mesh $(h_{\max})$. Parameters a and b (and error levels), for Equation (5.7) were obtained using the least squares data fitting method.

Figure 5.2 shows an example mesh used in computations consisting of 648 elements and 361 vertices. Furthermore, Figure 5.2 shows the fitted curves and the computed results. All of these results were computed with a constant CFL number (0.01). In this experiment, the low-storage Runge-Kutta (LSRK) time integration method was used. The data to which the fitting was applied were chosen so that hk was maximized for some polynomial order. All reported relative errors were computed at the final time instant $(t = 2)$ of the whole computational domain Ω. Table 5.2 lists the computed parameters a and b and also the error levels Δa and Δb.

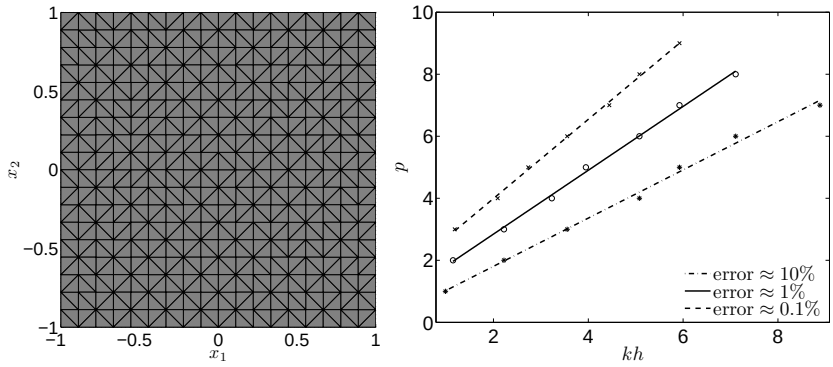

Figure 5.2: Left: An example computational mesh used in 2D computations including 648 elements and 361 vertices. Right: The polynomial order p as a function of the parameter hk for three relative error levels with a constant CFL number (0.01).

Table 5.2: Parameters $a \pm \Delta a$ and $b \pm \Delta b$ obtained using the least squares method. The first four lines apply to the 2D experiment and respectively last four lines to the 3D study.

2D	error $\approx 10\%$	error $\approx 1\%$	error $\approx 0.1\%$
a	0.7775	1.0294	1.2768
Δa	0.0243	0.0223	0.0211
b	0.2505	0.7857	1.4384
Δb	0.1326	0.1010	0.0822
3D			
a	1.4655	1.8498	2.3569
Δa	0.0705	0.0562	0.0516
b	0.0775	0.9040	1.3788
Δb	0.2279	0.1489	0.1183

Three-dimensional case

The domain for this experiment was a cube defined as $\Omega = [-1,\ 1]^3$. The PML was not used in this case. The normalized material parameters for Equation (3.1) were chosen so that wave speed $c = 1$, density $\rho = 1$, and absorption coefficient $\beta = 0$. The initial condition $\boldsymbol{u}(t = 0) = 0$. On the exterior boundary of the domain, an impedance-type boundary condition (2.21) with $Q = 0$ and $\sigma = 1/c$ was evaluated.

The analytic solution for the model problem is

$$\boldsymbol{u} = \begin{pmatrix} g(ct - \boldsymbol{k}\cdot\boldsymbol{x}) \\ -\boldsymbol{k}_1 g(ct - \boldsymbol{k}\cdot\boldsymbol{x}) \\ -\boldsymbol{k}_2 g(ct - \boldsymbol{k}\cdot\boldsymbol{x}) \\ -\boldsymbol{k}_3 g(ct - \boldsymbol{k}\cdot\boldsymbol{x}) \end{pmatrix}, \tag{5.8}$$

where $\boldsymbol{k} = (1, 0, 0)$. The source function g for Equation (2.24) was defined previously in Equation (5.6), with $f = 2$, $a_1 = -1$, and $t_0 = 0.75$.

In the 2D case, the mesh parameter h was chosen to be the maximum distance between two vertices in the element of the computational mesh. In the 3D case, mesh parameter h was computed as

$$h = \frac{1}{4}\sum_{\ell=1}^{4} |\boldsymbol{x}_{CM}^m - \boldsymbol{x}_\ell^m|\,, \tag{5.9}$$

where $\boldsymbol{x}_{CM}^m$ is the position of the centroid of arbitrary tetrahedron m and $\boldsymbol{x}_\ell^m, \ell = 1, \ldots, 4$ are the coordinates of the vertices.

Figure 5.3 shows an example uniform mesh, fitted curves, and computed results. All reported relative errors were computed at the final time instant $t = 2$ of the whole computational domain. The data fitting used in

this 3D example was evaluated with Equation (5.7) using the LSRK time integration scheme. All results were computed with a constant CFL number (0.001). As in the 2D case, the data to which the fitting was applied were chosen so that they were the maximum kh for some polynomial order. The relative error was computed at the final time instant $(t = 2)$ of the whole computational domain Ω. Values for fitted parameters a and b and also the error levels Δa and Δb are shown in Table 5.2.

A comparison of the 2D and 3D values for the fitted curves revealed that because different types of mesh parameter h were used, the values for the fitted curves cannot be directly compared. The values can, however, be compared with the factor of approximately 2.0, so that 2D values are smaller than 3D values. This phenomena can be explained by the different types of mesh parameter h.

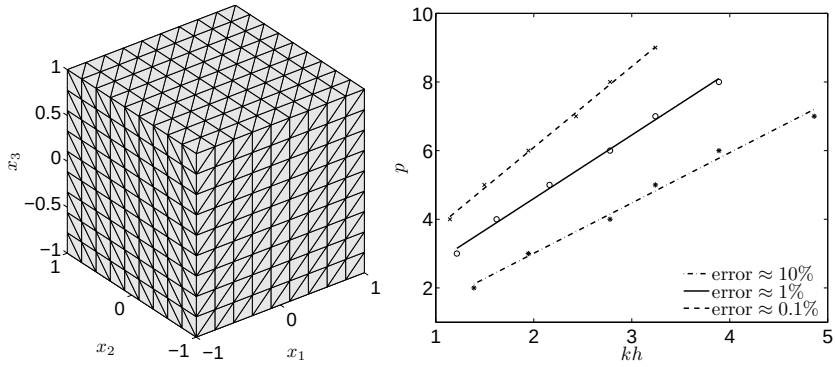

Figure 5.3: Left: An example of regularly refined tetrahedral mesh with 4374 elements and 1000 vertices. Right: The polynomial order p as a function of the parameter hk for three relative error levels with a CFL $= 0.001$.

5.1.3 Perfectly matched layer

To investigate the effect of several PML parameters, wave propagation was studied in a homogeneous medium. The domain for this example was a cube so that $\Omega = [-0.5 - \vartheta,\ 0.5 + \vartheta] \times [-0.5 - \vartheta,\ 0.5 + \vartheta] \times [-0.5 - \vartheta,\ 0.5 + \vartheta]$, where ϑ denotes the PML thickness. For this model problem, the normalized material parameters were chosen so that wave speed $c = 1$, density $\rho = 1$, and attenuation coefficient $\beta = 0$.

On the exterior boundary of the domain, an ABC (2.21) with $Q = 0$, $g = 0$, and $\sigma = 1/c$ was evaluated. In this model problem, the time span was from 0 to 3. The LSRK time-stepping method was used to approximate the time derivatives of system (3.5) with CFL $= 0.001$.

Figure 5.4 shows an example mesh used in the computations. The visualized grid contains 10015 tetrahedral elements, 2124 vertices, the minimum distance between two vertices $h_{\min} = 0.0858$, and respectively maximum distance between two vertices $h_{\max} = 0.3422$. The PML thickness ϑ was 0.4 in the visualized mesh. Figure 5.4 also shows the number of elements as a function of the polynomial degree p. The stipulated error level was 1.0% in the distribution shown. More details about the computational meshes used in this experiment are shown in Table 5.3.

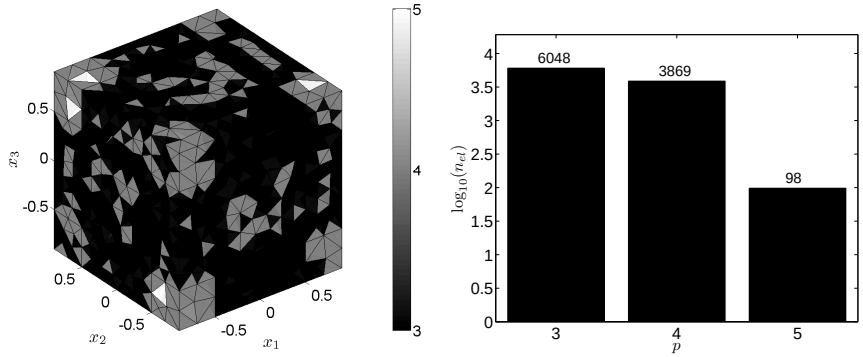

Figure 5.4: Left: An example mesh used in computations with 10015 elements and 2124 vertices. The gradient bar shows the polynomial order. Right: The number of elements $\log_{10}(n_{el})$ *as a function of the polynomial basis order p. The stipulated error level was* 1.0% *in this experiment. In the bar plot, the number over the bar shows the total value of the tetrahedral elements for each basis degree.*

In this experiment, sound was generated using an initial condition

$$\boldsymbol{u}(t=0) = \begin{pmatrix} \exp\left(-\alpha \sum_{\ell=1}^{3} (x_\ell - x_s)^2\right) \\ 0 \\ 0 \\ 0 \end{pmatrix},$$

where the parameter $\alpha = 40$ and the center position of the source $x_s = 0.15$. The pressure field is zero inside the PML domain at the first time instant $t = 0$. The "exact" solution is computed in domain $\Omega = [-4,\ 4] \times [-4,\ 4] \times [-4,\ 4]$ using a dense mesh with a constant polynomial order ($p = 7$). The mesh used for computing the "exact" solution consists of 56130 elements and 10771 vertices ($h_{\max} = 0.3946$ and $h_{\min} = 0.1023$).

Figure 5.5 simulates the relative error as a function of parameter d_0 using three different values for the PML thickness ($\vartheta = 0.2, 0.3$, and 0.4). The spatial position where the relative error is examined was $(-0.4, -0.4, 0.4)$.

We also simulated the relative error as a function of the power η with a mesh including 5646 elements and 1242 vertices, and the stipulated error level was 1.0%. The results predict that it is reasonable to use power $\eta = 2$ in all cases. The results predict that if the thickness ϑ of the PML is increased the value for parameter d_0 can be chosen more freely. For example, if we choose $\vartheta = 0.2$ the value for $d_0 \in [30,\ 60]$, but if we take $\vartheta = 0.4$ the suitable value for $d_0 \in [20,\ 90]$.

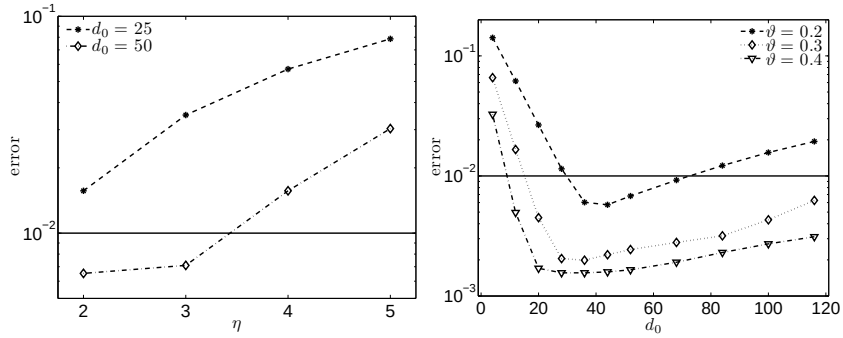

Figure 5.5: Left: The relative error as a function of power η for two values of d_0 with $\vartheta = 0.2$. Right: The relative error as a function of parameter d_0 for the three PML thicknesses ($\vartheta = 0.2, 0.3$, and 0.4). The solid line denotes the demanded 1.0% error level.

Table 5.3: The number of tetrahedral elements and vertices in meshes used in the computations, $h_{\min}$ denotes the shortest distance between two vertices in the mesh, $h_{\max}$ the longest distance between two vertices in the mesh, and ϑ is the thickness of the PML.

	mesh 1	mesh 2	mesh 3
elements	5646	7922	10015
vertices	1242	1717	2124
$h_{\min}$	0.1000	0.0963	0.0858
$h_{\max}$	0.3464	0.2942	0.3422
ϑ	0.2	0.3	0.4

5.2 APPLICATION EXAMPLE: SCATTERING FROM A CYLINDER

To demonstrate the effectiveness of the DG method and the parameter choices shown in Section 5.1, we performed a 3D experiment in which wave propagation was studied in a complex geometry. Here, the tweeter element of a loudspeaker was used as a sound source and wave scattering

from an infinitely long rigid cylinder was studied. The simulated wave field was compared to the measurements obtained in publication **IV**.

5.2.1 Computational model

In this model problem, wave propagation was studied in domain $\Omega = [-0.4\text{ m},\ 0.4\text{ m}] \times [-0.4675\text{ m},\ 0.3325\text{ m}] \times [-0.675\text{ m},\ 0.425\text{ m}]$. Domain Ω contains the PML layer and thickness $\vartheta = 20$ cm in each direction, surrounding the region of interest. Other PML parameters were chosen so that the decay parameter $d_0 = 50$ and power $\eta = 2$. Furthermore, a loudspeaker was used as a sound source and it was located at the region of interest. The geometry also contains an infinite long cylinder with radius $r = 3.5$ cm located at the origin towards the x_2-axis. Figure 5.6 shows the problem geometry.

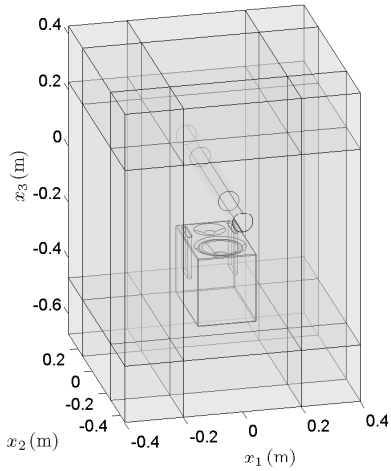

Figure 5.6: The problem geometry for the acoustic scattering example.

The propagation medium is air with the speed of sound $c = 343$ m/s and density $\rho = 1.21$ kg/m^3. Furthermore, here the attenuation coefficient β and the initial condition $\boldsymbol{u}(t = 0)$ are zero.

Boundary conditions for this model problem were chosen so that the tweeter element of the loudspeaker contains the inhomogeneous Neumann boundary condition (Equation (2.21) with $Q = -1$). The spatially independent sound source g is defined in Equation (5.10). The absorbing boundary condition with $Q = g = 0$ and $\sigma = 1/c$ was located at the external surface and also at the end of the reflex tubes. The homogeneous

$g = 0$ Neumann boundary condition $Q = -1$ was used on every other boundary of the loudspeaker and scattering cylinder.

The sound source for the model problem is a Gaussian pulse multiplied with the sine function. The source function is

$$g(t) = \exp\left(-\left(\gamma\left(t - t_0\right)\right)^2\right)\sin\left(\omega\left(t - t_0\right)\right), \tag{5.10}$$

where $\gamma = 6000$, t is the time, $t_0 = 0.5$ ms, and $\omega = 2\pi f$ denotes the angular frequency ($f = 10$ kHz). The time t spans from 0 to 2.0 ms. In this model problem, the CFL number is 0.001. The LSRK time integration method was used in this model problem.

The computational mesh for this example is shown in Figure 5.7. The same figure also shows the number of tetrahedral elements as a function of the polynomial basis order. The distribution is obtained with the stipulated error level 0.1%. The mesh consists of 85256 tetrahedral elements and 18109 vertices. The minimum distance between two vertices in the mesh is $h_{\min} = 0.24$ cm and the maximum distance $h_{\max} = 5.22$ cm.

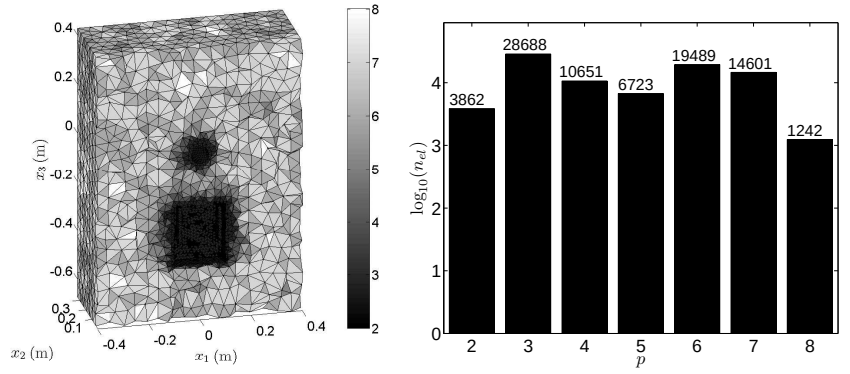

Figure 5.7: Left: The cross section of the mesh used in computations. Colorbar shows the order of the polynomial basis. Right: The number of tetrahedral elements n_{el} as a function of the polynomial order p. In the figure, the number over the bar shows the absolute value of the elements for the each p order. The distribution is obtained with the stipulated error level 0.1%.

Figure 5.8 shows the surface mesh of the loudspeaker and the scattering cylinder used in this experiment. The loudspeaker shown in 5.8 is a detailed approximation of the loudspeaker that was used for the measurements. For example, the model of the loudspeaker contains rounded corners for the main box of the loudspeaker. The surface of the loudspeaker is covered by mesh comprising 7444 triangle elements. Similarly,

the surface of the cylinder comprises 2176 triangles. In the surface visualization, the tweeter element is shown in a different color.

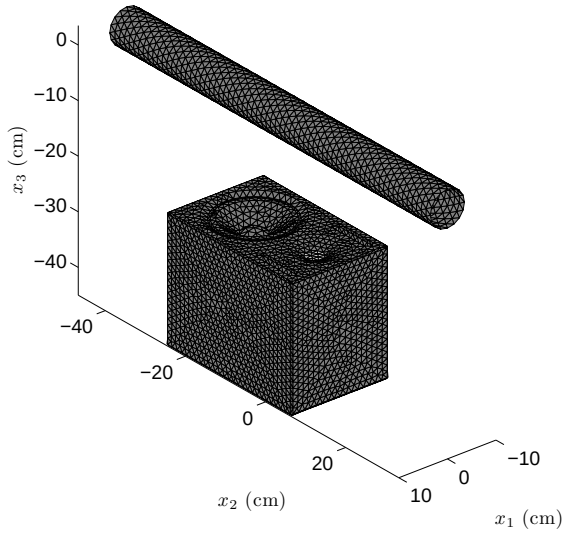

Figure 5.8: The surface mesh of the loudspeaker and scattering cylinder. In figure, the source surface (the tweeter element) is shown in a different color.

5.2.2 Measurement setup

The measurement system we used consisted of data acquisition hardware, a 3D positioning system, and measurement sensor. The measurement sensor was a single Brüel & Kjær free field microphone. Data acquisition hardware controlled both movements and measurements. The data acquisition hardware was manufactured by National Instruments.

The measurement procedure was as follows; first the sensor was placed in the initial position. The input signal (Equation (5.10)) was then fed to the loudspeaker and its response was measured. The sensor was then moved to the next position and the signal fed to the loudspeaker and its response measured again. This process was repeated until the entire measurement area was covered. For each measurement, the input signal was used as a triggering signal so that all measurement signals can be assumed to be captured simultaneously. After each movement, we waited a certain time to ensure that all vibrations from the movement were attenuated. This time was determined for each sensor before making measurements based on visual observation. All measurements were

performed in a semi-anechoic chamber.

5.2.3 Comparison between measurements and simulations

Figure 5.9 shows the normalized pressure amplitude as a function of time in two spatial positions. Point 1 $(x_1, x_2, x_3) = (0, 0, 4.5)$ cm is behind the cylinder 1 cm behind the surface of the cylinder. Point 2 $(x_1, x_2, x_3) = (5, 0, 4.5)$ cm is also behind the cylinder but 5 cm to the right from point 1 (towards the positive x_1-axis). Both points are in the same plane shown in Figure 5.10. Good agreement was obtained when the simulation was compared to the actual measurements. For example, the numerical method seems to model the diffraction accurately because the point where numerical and simulated results were compared is behind the scattering cylinder. On the other hand, the results show that the use of the sound-hard boundary condition on the surface of the cylinder is justified.

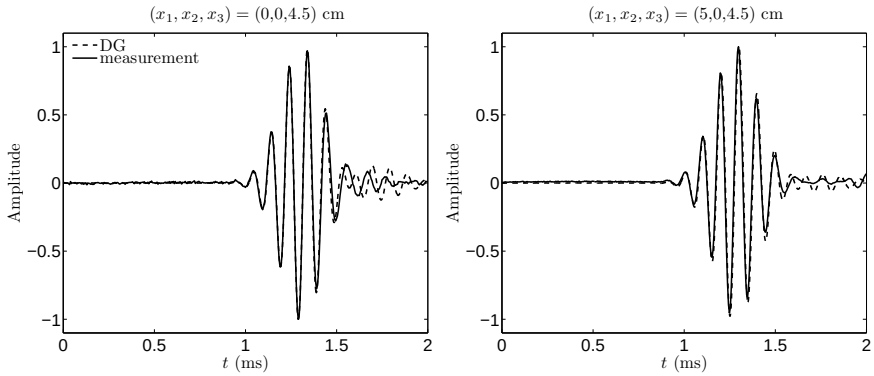

Figure 5.9: Normalized pressure amplitude for the simulated (dotted line) and measured (solid line) solutions as a function of time in two positions. Titles show the receiver position.

Figure 5.10 shows snapshots of the acoustic pressure fields. These snapshots were visualized at two time points, $t_1 = 0.90$ ms and $t_2 = 1.38$ ms. In both of these snapshots, the surface of the loudspeaker (gray) is also shown. The snapshots were chosen so that at the first time point $(t_1 = 0.90$ ms$)$ the incident field was completely generated from the tweeter element of the loudspeaker and, on the other hand, propagated at the scattering cylinder. In the second time instant $t_2 = 1.38$ ms the scattered field is generated from the cylinder. The second snapshot shows that the diffracted field is generated behind the cylinder and also fairly

behind the loudspeaker.

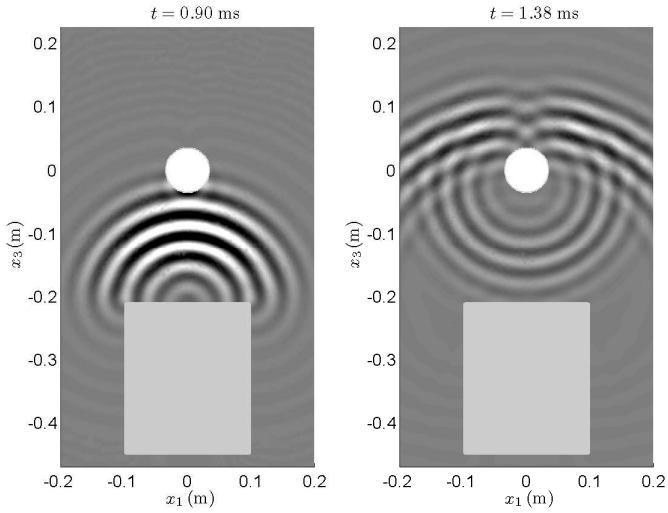

Figure 5.10: Snapshots of the pressure fields in two time instants.

5.3 DISCUSSION

This section discusses the numerical experiments shown in previous Sections 5.1 and 5.2. In Figure 5.1 the effect of the flux splitting parameter in publication **I** for the accuracy of the solution were studied. The results predict that the practical choice for the parameter σ is to use the value $\sigma = 1/c$, which corresponds to the case where the impedance-type boundary condition is used between adjacent elements in the computational mesh.

Non-uniform basis orders were one of the main research topics of this thesis. Section 5.1.2 was dedicated to the study of the basis order selection method provided in this thesis. With the non-uniform basis orders, the computational load can be reduced and, on the other hand, the benchmark problems studied in publications **II** and **III** predict that the stipulated error level is achieved.

The results shown in Figure 5.5 demonstrate the effect of the PML parameters on the accuracy of the solution. Based on these results, we developed guidelines from which the parameter values for the PML can be achieved. For example, it is reasonable to use the PML power parameter $\eta = 2$. One must note that the optimal PML parameter choices may be

different, for example, when solving wave propagation in elastic media versus in moving fluids.

In the application example, wave propagation was studied in complex 3D geometry in publication **IV**. The advantages of the non-uniform basis and the PML parameters were demonstrated in this model problem. Figure 5.8 shows the surface mesh of the loudspeaker. The figure shows that the geometric details on the surface of the loudspeaker are covered using small triangles. On the other hand, in the free space the mesh size increases. Based on these, the use of the non-uniform basis (Figure 5.7) is justified. The results (Figure 5.9) predict that tolerable agreement is achieved when comparing the simulated results with the actual measurements.

6 Conclusions

This thesis studied the feasibility of the DG method for large-scale modeling of time-domain acoustic problems. The previously proposed DG scheme [6] for time-domain acoustic problems in an inhomogeneous medium was analyzed numerically for 2D and 3D problems. In this thesis, the DG method was investigated from a computational point of view. The accuracy of the solution obtained using the DG method can be influenced in several ways, including the flux splitting, the order of the polynomial basis functions, the method used for truncating the computational domain, and the time integration approach.

Numerical flux plays an important role in the accuracy of the solution achieved using the DG method. The numerical flux used in this thesis was originally published in [89]. In the numerical experiments, we studied the effect of the flux coupling parameter on the accuracy of the solution. The results predicted that it is reasonable to use the flux coupling parameter, which was the mean value of the speed of sound on the interface of adjacent elements of the computational mesh.

The basis order affects the accuracy of the numerical approximation obtained using the DG method. In many realistic model problems, however, the mesh size parameter in the elements of the computational mesh is highly different. The use of a high-order polynomials with the DG method with small elements can cause instability [7]. One solution to overcome this problem is to use non-uniform basis order (known as the *p*-adaptivity). Based on previous theoretical studies, the non-uniform basis order was one of the main research topics of this thesis. The advantages of using the non-uniform basis are promising and worth using to test the method for choosing the basis order in problems beyond acoustics. A natural choice would be to investigate the propagation of electromagnetic waves (i.e., Maxwell's equations).

In several model problems it is reasonable to truncate a physically unbounded problem into a problem with a bounded domain. As it is well-known that the use of the original Engquist-Majda absorbing boundary condition [8] affects the accuracy of the solution, more sophisticated boundary treatment is essential. In the current work, we used the perfectly matched layer (PML) to truncate the computational domain. In the model problems, we studied the effect of several PML parameters on the accuracy of the solution. The results confirmed that with the correct parameter choices, the PML is an extremely useful tool for truncating the

wave without producing unwanted reflections.

The method used for the time integration has a great impact on the accuracy of the numerical solution. In this thesis project, the Runge-Kutta, Crank-Nicolson, low-storage Runge-Kutta, and fourth-order explicit, and singly diagonally implicit Runge-Kutta methods were used for approximating the time derivatives. The low-storage Runge-Kutta method was the most preferred method (of those used in this thesis) because less time was needed to achieve the final time and yet a large convergence order was obtained.

In the future, our goal is to extend the DG method to the atmospheric acoustics. In the field of atmospheric acoustics several physical phenomena will be investigated. These include the different models for the wave absorption, effects of the ground (the fluid-solid interaction), and refraction of the sound. In these problems, the dimensions of the computational domains are usually large which means that the overall computational load is easily intolerable. One possible method to decrease the computational load is to use the non-uniform basis order.

The non-linear wave problems are another application which will be considered in the future work. In this case, the main topic is to model the shock wave caused by a supersonic projectile. The shock front propagates as a function of time, which means that a more sophisticated hp-adaptation coupled with the DG solver will be needed.

References

[1] K. Yee, "Numerical solution of inital boundary value problems involving Maxwell's equations in isotropic media," *IEEE Transactions on Antennas and Propagation* **14,** 302–307 (1966).

[2] G. Cohen, *Higher-Order Numerical Methods for Transient Wave Equations* (Springer-Verlag, 2002).

[3] J. Simpson, R. Heikes, and A. Taflove, "FDTD modeling of a novel ELF radar for major oil deposits using a three-dimensional geodesic grid of the earth-ionosphere waveguide," *IEEE Transactions on Antennas and Propagation* **54,** 1734–1741 (2006).

[4] F. Marquet, M. Pernot, J.-F. Aubry, G. Montaldo, L. Marsac, M. Tanter, and M. Fink, "Non-invasive transcranial ultrasound therapy based on a 3D CT scan: Protocol validation and *in vitro* results," *Physics in Medicine and Biology* **54,** 2597–2613 (2009).

[5] P. Monk, *Finite Element Methods for Maxwell's Equations* (Clarendon Press, Oxford, 2003).

[6] W. Reed and T. Hill, *Triangular mesh methods for the neutron transport equation* (Technical report, Los Alamos National Laboratory, Los Alamos, New Mexico, USA, LA-UR-73-479, 1973).

[7] J. Hesthaven and T. Warburton, *Nodal Discontinuous Galerkin Methods: Algorithms, Analysis, and Applications* (Springer, 2007).

[8] B. Engquist and A. Majda, "Absorbing boundary conditions for the numerical simulation of waves," *Mathematics of Computation* **31,** 629–651 (1977).

[9] J.-P. Bérenger, "A perfectly matched layer for the absorption of electromagnetic waves," *Journal of Computational Physics* **114,** 185–200 (1994).

[10] B. Cockburn and C.-W. Shu, "The Runge-Kutta local projection P^1-discontinuous Galerkin method for scalar conservation laws," *RAIRO Mathematical Modelling and Numerical Analysis* **25,** 337–361 (1991).

[11] A. Jameson, H. Schmidt, and E. Turkel, "Numerical solution of the Euler equations by finite volume methods using Runge-Kutta time-stepping schemes," *AIAA paper* (1981).

[12] A. Kanevsky, M. Carpenter, D. Gottlieb, and J. Hesthaven, "Application of implicit-explicit high order Runge-Kutta methods to discontinuous-Galerkin schemes," *Journal of Computational Physics* **225,** 1753–1781 (2007).

[13] C. Kennedy and M. Carpenter, "Additive Runge-Kutta schemes for convection-diffusion-reaction equations," *Applied Numerical Mathematics* **44,** 139–181 (2003).

[14] M. Grote, A. Schneebeli, and D. Schötzau, "Discontinuous Galerkin finite element method for the wave equation," *SIAM Journal on Numerical Analysis* **44,** 2408–2431 (2006).

[15] E. Toro, R. Millington, and L. Nejad, "Towards very high order Godunov schemes," in *Godunov Methods: Theory and Applications*, E. Toro, ed. (Kluwer Academic Publishers, 2001).

[16] V. Titarev and E. Toro, "ADER: Arbitrary high order Godunov approach," *Journal of Scientific Computing* **17,** 609–618 (2002).

[17] F. Hu, "A stable, perfectly matched layer for linearized Euler equations in unsplit physical variables," *Journal of Computational Physics* **173,** 455–480 (2001).

[18] P. Filippi, D. Habault, J. Lefebvre, and A. Bergassoli, *Acoustics: Basic Physics, Theory and Methods* (Academic Press, 1999).

[19] A. Pierce, *Acoustics: An Introduction to Its Physical Principles and Applications* (The Acoustical Society of America, 1981).

[20] L. Kinsler, A. Frey, A. Coppens, and J. Sanders, *Fundamentals of Acoustics* (John Wiley & Sons, 1999).

[21] R. Leveque, *Finite Volume Method for Hyperbolic Problems* (Cambridge University Press, 2002).

[22] F. Ihlenburg and I. Babuška, "Dispersion analysis and error estimation of Galerkin finite element methods for the Helmholtz equation," *International Journal for Numerical Methods in Engineering* **38,** 3745–3774 (1995).

[23] F. Ihlenburg and I. Babuška, "Finite element solution of the Helmholtz equation with high wave number part I: The h-version of the FEM," *Computers Mathematics with Applications* **30,** 9–37 (1995).

[24] F. Ihlenburg and I. Babuška, "Finite element solution of the Helmholtz equation with high wave number part II: The h-p version of the FEM," *SIAM Journal on Numerical Analysis* **34,** 315–358 (1997).

[25] F. Ihlenburg, *Finite Element Analysis of Acoustic Scattering* (Springer, 1998).

[26] I. Babuška and S. Sauter, "Is the pollution effect on the FEM avoidable for the Helmholtz equation considering high wave numbers?," *SIAM Journal of Numerical Analysis* **34,** 2392–2432 (1997).

[27] A. Quarteroni, R. Sacco, and F. Salieri, *Numerical Mathematics* (Springer, 2000).

[28] M. Dumbser, M. Käser, and E. Toro, "An arbitrary high-order Discontinuous Galerkin method for elastic waves on unstructured meshes - V. Local time stepping and *p*-adaptivity," *Geophysical Journal International* **171,** 695–717 (2007).

[29] R. Courant, K. Friedrichs, and H. Lewy, "Über die partiellen differenzengleichungen der mathematischen," *Mathematische Annalen* **100,** 32–74 (1928).

[30] R. Courant, K. Friedrichs, and H. Lewy, "On the partial difference equations of mathematical physics," *IBM Journal* 215-234 (1967).

[31] S. Leeman, L. Hutchins, and J. Jones, "Bounded pulse propagation," *Acoustical Imaging* **10,** 427–435 (1982).

[32] T. Szabo, "Time domain wave equations for lossy media obeying a frequency power law," *The Journal of the Acoustical Society of America* **96,** 491–500 (1994).

[33] S. Leeman, L. Hutchins, and J. Jones, "Pulse scattering in dispersive media," *Acoustical Imaging* **11,** 139–147 (1982).

[34] T. Szabo, "Causal theories and data for acoustic attenuation obeying a frequency power law," *The Journal of the Acoustical Society of America* **97,** 14–24 (1995).

[35] R. Cobbold, N. Sushilov, and A. Weathermon, "Transient propagation in media with classical or power-law loss," *The Journal of the Acoustical Society of America* **116,** 3294–3303 (2004).

[36] K. Friedrichs, "Symmetric positive linear differential equations," *Communications on Pure and Applied Mathematics* **11,** 333–418 (1958).

[37] A. Krokstad, S. Strom, and S. Sørsdal, "Calculating the acoustical room response by the use of a ray tracing technique," *Journal of Sound and Vibration* **8,** 118–125 (1968).

[38] G. Liang and H. Bertoni, "A new approach to 3-D ray tracing for propagation prediction in cities," *IEEE Transactions on Antennas and Propagation* **46,** 853–863 (1998).

[39] G. Durgin, N. Patwari, and T. Rappaport, "Improved 3D ray launching method for wireless propagation prediction," *Electronics Letters* **33,** 1414–1413 (1997).

[40] J. Carrer, W. Mansur, and R. Vanzuit, "Scalar wave equation by the boundary element method: A D-BEM approach with non-homogeneous initial conditions," *Computational Mechanics* **44,** 31–44 (2009).

[41] P. Banerjee and R. Butterfield, *Boundary Element Methods in Engineering Science* (McGraw-Hill, 1994).

[42] G. Beer, *Programming the Boundary Element Method: An Introduction for Engineers* (John Wiley & Sons, 2001).

[43] M. Dougherty and R. Stephen, "Geoacoustic scattering from seafloor features in the ROSE area," *The Journal of the Acoustical Society of America* **82,** 238–256 (1987).

[44] A. Taflove and K. Umashankar, "Review of FD-TD numerical modeling of electromagnetic wavescattering and radar cross section," *Proceedings of the IEEE* **77,** 682–699 (1989).

[45] W.-F. Chang and G. McMechan, "Absorbing boundary conditions for 3-D acoustic and elastic finite-difference calculations," *Bulletin of the Seismological Society of America* **79,** 211–218 (1989).

[46] I. Hallaj, R. Cleveland, and K. Hynynen, "Simulations of the thermo-acoustic lens effect during focused ultrasound surgery," *The Journal of the Acoustical Society of America* **109,** 2245–2253 (2001).

[47] C. Connor and K. Hynynen, "Bio-acoustic thermal lensing and nonlinear propagation in focused ultrasound surgery using large focal spots: A parametric study," *Physics in Medicine and Biology* **47,** 1911–1929 (2002).

[48] H. Versteeg and W. Malalasekra, *An Introduction to Computational Fluid Dynamics: The Finite Volume Method* (Prentice Hall, 2007).

[49] S. Piperno, M. Remaki, and L. Fezoui, "A nondiffusive finite volume scheme for the three-dimensional Maxwell's equations on unstructured meshes," *SIAM Journal on Numerical Analysis* **39,** 2089–2108 (2001).

[50] J. Cioni, L. Fezoui, H. Steve, J.-P. Cioni, and L. Fezoui, "A parallel time-domain Maxwell solver using upwind schemes and triangular meshes," *IMPACT of Computing in Science and Engineering* **5,** 215–247 (1993).

[51] T. Moroney and I. Turner, "A three-dimensional finite volume method based on radial basis functions for the accurate computational modelling of nonlinear diffusion equations," *Journal of Computational Physics* **225,** 1409–1426 (2007).

[52] G. Cohen, P. Joly, J. Roberts, and N. Tordjman, "Higher order triangular finite elements with mass lumping for the wave equation," *SIAM Journal on Numerical Analysis* **38,** 2047–2078 (2001).

[53] S. Jund and S. Salmon, "Arbitrary high-order finite element schemes and high-order mass lumping," *International Journal of Applied Mathematics and Computer Sciences* **17,** 375–393 (2007).

[54] S. Pernet, X. Ferrieres, and G. Cohen, "High spatial order finite element method to solve Maxwell's equations in time domain," *IEEE Transactions on Antennas and Propagation* **53,** 2889–2899 (2005).

[55] C. Ma, "Finite-element method for time-dependent Maxwell's equations based on an explicit-magnetic-field scheme," *Journal of Computational and Applied Mathematics* **194,** 409–424 (2006).

[56] J. Li, "Error analysis of finite element methods for 3-D Maxwell's equations in dispersive media," *Journal of Computational and Applied Mathematics* **188,** 107–120 (2006).

[57] O. Zienkiewicz and R. Taylor, *The Finite Element Method: Solid Mechanics* (Butterworth-Heinemann, 2000).

[58] B.-N. Jiang and G. Carey, "Least-squares finite element methods for compressible Euler equations," *International Journal for Numerical Methods in Fluids* **10,** 557–568 (2005).

[59] L. Thompson, "A review of finite-element methods for time-harmonic acoustics," *The Journal of the Acoustical Society of America* **119,** 1315–1330 (2006).

[60] F. Collino, "High order absorbing boundary conditions for wave propagation models: Straight line boundary and corner cases," in *Mathematical and Numerical Aspects of Wave Propagation* (1993), pp. 161–171.

[61] M. Grote and J. Geller, "Exact nonreflecting boundary conditions for the time dependent wave equation," *SIAM Journal on Applied Mathematics* **55,** 280–297 (1995).

[62] M. Grote and J. Geller, "Nonreflecting boundary conditions for time-dependent scattering," *Journal of Computational Physics* **127,** 52–65 (1996).

[63] D. Givoli, "High-order non-reflecting boundary conditions without high-order derivatives," *Journal of Computational Physics* **170,** 849–870 (2001).

[64] D. Givoli and B. Neta, "High-order non-reflecting boundary scheme for time-dependent waves," *Journal of Computational Physics* **186,** 24–46 (2003).

[65] J. Diaz and P. Joly, "A time domain analysis of PML models in acoustics," *Computer Methods in Applied Mechanics and Engineering* **195,** 3820–3853 (2006).

[66] F. Collino and P. Monk, "Optimizing the perfectly matched layer," *Computer Methods in Applied Mechanics and Engineering* **164,** 157–171 (1998).

[67] E. Bécache, P. Petropoulos, and S. Gedney, "On the long-time behavior of unsplit perfectly matched layers," *IEEE Transactions on Antennas and Propagation* **52,** 1335–1342 (2004).

[68] S. Abarbanel and D. Gottlieb, "On the construction and analysis of absorbing layers in CEM," *Applied Numerical Mathematics* **27,** 331–340 (1998).

[69] S. Abarbanel, D. Gottlieb, and J. Hesthaven, "Well-posed perfectly matched layers for advective acoustics," *Journal of Computational Physics* **154,** 266–283 (1999).

[70] W. Chew and W. Weedon, "A 3D perfectly matched medium from modified Maxwell's equations with stretched coordinates," *Microwave and Optical Technology Letters* **7,** 599–604 (1994).

[71] B. Cockburn and C.-W. Shu, "TVB Runge-Kutta local projection discontinuous Galerkin finite element method for scalar conservation laws II: General framework," *Mathematics of Computation* **52,** 411–435 (1989).

[72] M. Carpenter and C. Kennedy, *Fourth-order 2N-storage Runge-Kutta schemes* (Technical report, NASA-TM-109112, 1994).

[73] A. Gerisch and R. Weiner, "The positivity of low-order explicit Runge-Kutta schemes applied in splitting methods," *Computers & Mathematics with Applications* **45,** 53–67 (2003).

[74] M. Calvo, J. Franco, and L. Randez, "A new minimum storage Runge-Kutta scheme for computational acoustics," *Journal of Computational Physics* **201,** 1–12 (2004).

[75] A. Catella, V. Dolean, and S. Lanteri, *An implicit DGTD method for solving the two-dimensional Maxwell equations on unstructured triangular meshes* (Technical report, INRIA, 2006).

[76] T. Schwartzkopff, C. Munz, and E. Toro, "ADER: A high-order approach for linear hyperbolic systems in 2D," *Journal of Scientific Computing* **17,** 231–240 (2002).

[77] V. Titarev and E. Toro, "ADER schemes for three-dimensional nonlinear hyperbolic systems," *Journal of Computational Physics* **204,** 715–736 (2005).

[78] M. Käser and M. Dumbser, "An arbitrary high-order discontinuous Galerkin method for elastic waves on unstructured meshes - I. The two-dimensional isotropic case with external source terms," *Geophysical Journal International* **166,** 855–877 (2006).

[79] M. Dumbser and M. Käser, "An arbitrary high-order discontinuous Galerkin method for elastic waves on unstructured meshes - II. The three-dimensional isotropic case," *Geophysical Journal International* **167,** 319–336 (2006).

[80] J. de la Puente, M. Käser, M. Dumbser, and H. Igel, "An arbitrary high-order discontinuous Galerkin method for elastic waves on unstructured meshes - IV. Anisotropy," *Geophysical Journal International* **169,** 1210–1228 (2007).

[81] M. Käser, M. Dumbser, J. de la Puente, and H. Igel, "An arbitrary high-order discontinuous Galerkin method for elastic waves on unstructured meshes - III. Viscoelastic attenuation," *Geophysical Journal International* **168,** 224–242 (2007).

[82] M. Käser, C. Castro, V. Hermann, J. de la Puente, and C. Pelties, "Recent Developments of the ADER-discontinuous Galerkin scheme for computational seismology: A critical view on its advantages and disadvantages," in *The 9th International Conference on Mathematical and Numerical Aspects of Waves Propagation* (2009), pp. 68–69.

[83] J. Flaherty, R. Loy, M. Shephard, B. Szymanski, J. Teresco, and L. Ziantz, "Adaptive local refinement with octree load balancing for the parallel solution of three-dimensional conservation laws," *Journal of Parallel and Distributed Computing* **47,** 139–152 (1997).

[84] S. Piperno, "Symplectic local time-stepping in non-dissipative DGTD methods applied to wave propagation problems," *Mathematical Modelling and Numerical Analysis* **40,** 815–841 (2006).

[85] A. Taube, M. Dumbser, C.-D. Munz, and R. Schneider, "A high-order discontinuous Galerkin method with time-accurate local time stepping for the Maxwell equations," *International Journal of Numerical Modelling: Electronic Networks, Devices and Fields* **22,** 77–103 (2009).

[86] G. Richter, "An explicit finite element method for the wave equation," *Applied Numerical Mathematics* **16,** 65–80 (1994).

[87] R. Lowrie, P. Roe, and B. van Leer, "A space-time discontinuous Galerkin method for the time-accurate numerical solution of hyperbolic conservation laws," in *Collection of Technical Papers* (AIAA Computational Fluid Dynamics Conference, 1995).

[88] O. Karakashian and C. Makridakis, "A space-time finite element method for the nonlinear Schrödinger equation: The discontinuous Galerkin method," *Mathematics of Computation* **67,** 479–499 (1998).

[89] P. Monk and G. Richter, "A discontinuous Galerkin method for linear symmetric hyperbolic systems in inhomogeneous media," *Journal of Scientific Computing* **22-23,** 443–477 (2005).

[90] B. Cockburn, G. Karniadakis, and C.-W. Shu, eds., *Discontinuous Galerkin Methods Theory, Computation and Applications* (Springer, 2000).

[91] J. van der Vegt and H. van der Ven, "Space-time discontinuous Galerkin finite element method with dynamic grid motion for inviscid compressible flows: I. General formulation," *Journal of Computational Physics* **182,** 546–585 (2002).

[92] B. Cockburn, "Discontinuous Galerkin methods for convection-dominated problems," in *High-Order Methods for Computational Physics*, T. Barth and H. Deconinck, eds. (Springer-Verlag, 1999), pp. 69-224.

[93] Y. Xu and C.-W. Shu, "Local discontinuous Galerkin methods for high-order time-dependent partial differential equations," *Communications in Computational Physics* **7,** 1–46 (2010).

[94] G. Cohen, X. Ferrieres, and P. Pernet, "A spatial high-order hexahedral discontinuous Galerkin method to solve Maxwell's equations in time domain," *Journal of Computational Physics* **217,** 340–363 (2006).

[95] J. Hesthaven and T. Warburton, "Nodal high-order methods on unstructured grids I. Time-domain solution of Maxwell's equations," *Journal of Computational Physics* **181,** 186–221 (2002).

[96] B. Cockburn, F. Li, and C.-W. Shu, "Locally divergence-free discontinuous Galerkin methods for the Maxwell equations," *Journal of Computational Physics* **194,** 588–610 (2004).

[97] M. Grote, A. Schneebeli, and D. Schötzau, "Interior penalty discontinuous Galerkin method for Maxwell's equations: Energy norm error estimates," *Journal of Computational and Applied Mathematics* **204,** 375–386 (2007).

[98] T. Lu, W. Cai, and P. Zhang, "Discontinuous Galerkin time-domain method for GPR simulation in dispersive media," *IEEE Transactions on Geoscience and Remote Sensing* **43,** 72–80 (2005).

[99] M. Käser and M. Dumbser, "A highly accurate discontinuous Galerkin method for complex interfaces between solids and moving fluids," *Geophysics* **73,** 23–35 (2008).

[100] F. Giraldo, J. Hesthaven, and T. Warburton, "Nodal high-order discontinuous Galerkin methods for the spherical shallow water equations," *Journal of Computational Physics* **181,** 499–525 (2002).

[101] C. Dawson and V. Aizinger, "A discontinuous Galerkin method for three-dimensional shallow water equations," *Journal of Scientific Computing* **22-23,** 245–267 (2005).

[102] C. Eskilsson and S. Sherwin, "Discontinuous Galerkin spectral/hp element modelling of dispersive shallow water systems," *Journal of Scientific Computing* **22-23,** 269–288 (2005).

[103] K. Shahbazi, P. Fischer, and C. Ethier, "A high-order discontinuous Galerkin method for the unsteady incompressible Navier-Stokes equations," *Journal of Computational Physics* **222,** 391–407 (2007).

[104] F. Bassi and S. Rebay, "A high-order accurate discontinuous finite element method for the numerical solution of the compressible Navier-Stokes equations," *Journal of Computational Physics* **131,** 267–279 (1997).

[105] B. Cockburn, G. Kanschat, and D. Schötzau, "A locally conservative LDG method for the incompressible Navier-Stokes equations," *Mathematics of Computation* **74,** 1067–1095 (2005).

[106] G. Lin and G. Karniadakis, "A discontinuous Galerkin method for two-temperature plasmas," *Computer Methods in Applied Mechanics and Engineering* **195,** 3504–3527 (2006).

[107] J. Loverich and U. Shumlak, "A discontinuous Galerkin method for the full two-fluid plasma model," *Computer Physics Communications* **169,** 251–255 (2005).

[108] A. Klöckner, T. Warburton, J. Bridge, and J. Hesthaven, "Nodal discontinuous Galerkin methods on graphics processors," *Journal of Computational Physics* **228,** 7863–7882 (2009).

[109] R. Falk and G. Richter, "Explicit finite element methods for symmetric hyperbolic equations," *SIAM Journal on Numerical Analysis* **36,** 935–952 (1999).

[110] D. Arnold, F. Brezzi, B. Cockburn, and L. Marini, "Unified analysis of discontinuous Galerkin methods for elliptic problems," *SIAM Journal on Numerical Analysis* **39,** 1749–1779 (2001).

[111] A. Harten, P. Lax, and B. van Leer, "On upstream differencing and Godunov-type Schemes for hyperbolic conservation laws," *SIAM Review* **25,** 35–61 (1983).

[112] J. Qiu, B. Khoo, and C.-W. Shu, "A numerical study for the performance of the Runge-Kutta discontinuous Galerkin method based on different numerical fluxes," *Journal of Computational Physics* **212,** 540–565 (2006).

[113] R. Kirby and G. Karniadakis, "Selecting the numerical flux in discontinuous Galerkin methods for diffusion problems," *Journal of Scientific Computing* **22-23,** 385–411 (2005).

[114] G. Karniadakis and S. Sherwin, *Spectral/hp Element Methods for CFD* (Oxford University Pres, 1999).

[115] Q. Chen and I. Babuška, "Approximate optimal points for polynomial interpolation of real functions in an interval and in a triangle,"

Computer Methods in Applied Mechanics and Engineering **128,** 405–417 (1995).

[116] J. Hesthaven, "From electrostatics to almost optimal nodal sets for polynomial interpolation in a simplex," *SIAM Journal on Numerical Analysis* **35,** 655–676 (1998).

[117] J. Hesthaven and C. Teng, "Stable spectral methods on tetrahedral elements," *SIAM Journal on Scientific Computing* **21,** 2352–2380 (1999).

[118] Q. Chen and I. Babuška, "The optimal symmetrical points for polynomial interpolation of real functions in the tetrahedron," *Computer Methods in Applied Mechanics and Engineering* **137,** 89–94 (1996).

[119] G. Gabard, "Discontinuous Galerkin methods with plane waves for the displacement-based acoustic equation," *International Journal for Numerical Methods in Engineering* **66,** 549–569 (2006).

[120] G. Gabard, "Discontinuous Galerkin methods with plane waves for time-harmonic problems," *Journal of Computational Physics* **225,** 1961–1984 (2007).

[121] C. Farhat, I. Harari, and U. Hetmaniuk, "A discontinuous Galerkin method with Lagrange multipliers for the solution of Helmholtz problems in the mid-frequency regime," *Computer Methods in Applied Mechanics and Engineering* **192,** 1389–1419 (2003).

[122] T. Huttunen, P. Monk, and J. Kaipio, "Computational aspects of the ultra-weak variational formulation," *Journal of Computational Physics* **182,** 27–46 (2002).

[123] T. Huttunen, M. Malinen, and P. Monk, "Solving Maxwell's equations using the ultra weak variational formulation," *Journal of Computational Physics* **223,** 731–758 (2007).

[124] B. Després, "Sur une formulation variationnelle de type ultra-faible," *Comptes Rendus de l'Academie des Sciences - Series I* **318,** 939–944 (1994).

[125] O. Cessenat and B. Després, "Application of an ultra weak variational formulation of elliptic PDEs to the two-dimensional Helmholtz problem," *SIAM Journal of Numerical Analysis* **35,** 255–299 (1998).

[126] O. Cessenat and B. Després, "Using plane waves as base functions for solving time harmonic equations with the ultra weak variational formulation," *Journal of Computational Acoustics* **11,** 227–238 (2003).

[127] T. Huttunen, J. Kaipio, and P. Monk, "The perfectly matched layer for the ultra weak variational formulation of the 3D Helmholtz problem," *International Journal for Numerical Methods in Engineering* **61,** 1072–1092 (2004).

[128] T. Huttunen, P. Monk, F. Collino, and J. Kaipio, "The ultra weak variational formulation for elastic wave problems," *SIAM Journal on Scientific Computing* **25,** 1717–1742 (2004).

[129] T. Huttunen, J. Kaipio, and P. Monk, "An ultra-weak method for acoustic fluidsolid interaction," *Journal of Computational and Applied Mathematics* **23,** 166–185 (2008).

[130] P. LeSaint and P. Raviart, "On a finite element method for solving the neutron transport equation," in *Mathematical Aspects of Finite Element Methods in Partial Differential Equations* (Academic Press, New York, 1974), pp. 89-123.

[131] C. Johnson and J. Pitkäranta, "An analysis of the discontinuous Galerkin method for a scalar hyperbolic equation," *Mathematics of Computation* **46,** 1–26 (1986).

[132] G. Richter, "An optimal-order error estimate for the discontinuous Galerkin method," *Mathematics of Computations* **50,** 75–88 (1988).

[133] G. Chavent and B. Cockburn, "The local projection P^0P^1 discontinuous- Galerkin finite element method for scalar conservation laws," *RAIRO Mathematical Modelling and Numerical Analysis* **23,** 565–592 (1989).

[134] B. Cockburn, S. Lin, and C.-W. Shu, "TVB Runge-Kutta local projection discontinuous Galerkin finite element method for conservation laws III: One-dimensional systems," *Journal of Computational Physics* **84,** 90–113 (1989).

[135] B. Cockburn, B. Hou, and C.-W. Shu, "TVB Runge-Kutta local projection discontinuous Galerkin finite element method for conservation laws IV: The multidimensional case," *Mathematics of Computation* **54,** 545–581 (1990).

[136] B. Cockburn and C.-W. Shu, "The Runge-Kutta local projection discontinuous Galerkin finite element method for conservation laws V: Multidimensional system," *Journal of Computational Physics* **141,** 199–224 (1998).

[137] F. Hu, M. Hussaini, and P. Rasetarinera, "An analysis of the discontinuous Galerkin method for wave propagation problems," *Journal of Computational Physics* **151,** 921–946 (1999).

[138] M. Ainsworth, "Dispersive and dissipative behaviour of high order discontinuous Galerkin finite element methods," *Journal of Computational Physics* **198,** 106–130 (2004).

[139] M. Ainsworth, P. Monk, and W. Muniz, "Dispersive and dissipative properties of the discontinuous Galerkin finite element methods for second-order wave equation," *Journal of Scientific Computing* **27,** 5–40 (2006).

[140] G. Karypis and V. Kumar, "A fast and high quality multilevel scheme for partitioning irregular graphs," *SIAM Journal on Scientific Computing* **20,** 359–392 (1998).

[141] K. Bey, A. Patra, and J. Oden, "A parallel *hp*-adaptive discontinuous Galerkin method for hyperbolic conservation laws," *Applied Numerical Mathematics* **20,** 321–336 (1996).

[142] K. Bey, A. Patra, and J. Oden, "*hp*-version discontinuous Galerkin methods for hyperbolic conservation laws: A parallel adaptive strategy," *International Journal for Numerical Methods in Engineering* **38,** 3889–3908 (2005).

[143] R. Biswas, K. Devine, and J. Flaherty, "Parallel, adaptive finite element methods for conservation laws," *Applied Numerical Methods* **14,** 255–283 (1994).

[144] K. Devine and J. Flaherty, "Parallel adaptive *hp*-refinement techniques for conservation laws," *Applied Numerical Mathematics* **20,** 367–386 (1996).

[145] J. Flaherty, L. Krivodonova, J.-F. Remacle, and M. Shephard, "Aspects of discontinuous Galerkin methods for hyperbolic conservation laws," *Finite Elements in Analysis and Design* **38,** 889–908 (2002).

[146] P.-E. Bernard, N. Chevaugeon, V. Legat, E. Deleersnijder, and J.-F. Remacle, "High-order *h*-adaptive discontinuous Galerkin methods for ocean modelling," *Ocean Dynamics* **57,** 109–121 (2007).

[147] P. Houston, B. Senior, and E. Süli, "*hp*-Discontinuous Galerkin finite element methods for hyperbolic problems: Error analysis and adaptivity," *International Journal for Numerical Methods in Fluids* **40,** 153–169 (2002).

Timo Lähivaara

Discontinuous Galerkin Method for Time-Domain Wave Problems

During the last decade there has been a rapid development of accurate, robust, and flexible computational techniques for modeling of complex wave dominated problems. One of the prominent areas of activity has been the study of electromagnetic, elasticity, and acoustic problems.

In this thesis, the high-order accurate discontinuous Galerkin (DG) method with the application to problems of wave propagation in acoustic and elastic media is studied.

Thesis addresses not only the development of DG method but also includes a discussion of other important numerical issues related to wave problems such as absorbing layers and efficient means of time integration.

UNIVERSITY OF
EASTERN FINLAND

Publications of the University of Eastern Finland
Dissertations in Forestry and Natural Sciences

ISBN 978-952-61-0239-9